

A three-dimensional, histological and deformable atlas of the human basal ganglia. I. Atlas construction based on immunohistochemical and MRI data

Jérôme Yelnik,^{a,b,c,*} Eric Bardinnet,^{d,e} Didier Dormont,^{d,f} Grégoire Malandain,^e
Sébastien Ourselin,^e Dominique Tandé,^{a,b,c} Carine Karachi,^{a,b,c,g} Nicholas Ayache,^e
Philippe Cornu,^g and Yves Agid^{a,b,c,h,i}

^aINSERM U679, Neurologie et Thérapeutique Expérimentale, Paris, France

^bHôpital de la Salpêtrière, Paris, France

^cUniversité Pierre et Marie Curie, Faculté de Médecine, Paris, France

^dCNRS UPR640–LENA, Paris, France

^eProjet Epidaure, INRIA, Sophia–Antipolis, France

^fDépartement de Neuroradiologie, CHU Pitié–Salpêtrière, Paris, France

^gDépartement de Neurochirurgie, CHU Pitié–Salpêtrière, Paris, France

^hCentre d'Investigation Clinique, CHU Pitié–Salpêtrière, Paris, France

ⁱFédération de Neurologie, CHU Pitié–Salpêtrière, Paris, France

Received 9 August 2005; revised 13 July 2006; accepted 19 September 2006

Available online 15 November 2006

This paper describes the construction of an atlas of the human basal ganglia. The successive steps of the construction were as follows. First a postmortem specimen was subjected to a MRI acquisition prior to extraction of the brain from the skull. The brain was then cryosectioned (70 μm thickness). One section out of ten (80 sections) was Nissl-stained with cresyl violet, another series of 80 sections was immunostained for the calcium binding protein calbindin. Contours of basal ganglia nuclei including their calbindin-stained functional subdivisions, fiber bundles and ventricles ($n=80$ structures) were traced from histological sections and digitized. A novelty of this atlas is the MRI acquisition, which represents the core data element of the study. MRI was used for the coregistration of the atlas data and permitted, through multimodal (Nissl, calbindin, images of cryosectioning, T1 and T2 MRI) and 3D optimization, the production of anatomically and geometrically consistent 3D surfaces, which can be sliced through any desired orientation. The atlas MRI is also used for its deformation to provide accurate conformation to the MRI of living patients, thus adding information at the histological level to the patient's MRI volume. This latter aspect will be presented in a forthcoming paper.

© 2006 Elsevier Inc. All rights reserved.

Introduction

This paper describes the construction of an atlas of the human basal ganglia. The atlas was developed in the clinical context of deep

brain stimulation (DBS) for the identification of deep brain structures of individual patients, but it is thought to be applicable to any research experiment involving brain imaging. With this goal in mind, the atlas has been conceived as a set of three dimensional (3D) histological structures that can be deformed to fit the brains of different patients.

Identification of deep brain structures in individual patients is crucial for the clinical and cognitive neuroscience communities who often demand a histological level of resolution. Stereotactic neurosurgery, intracerebral grafting and/or infusion of pharmacological agents are domains in which a high degree of accuracy is required. A particularly important field is that of DBS, first proposed for the treatment of tremor (Benabid et al., 1987) and for which the precise localization of the target has proved to be a critical prerequisite condition. The target for DBS in Parkinson's disease has been moved from the thalamus to the globus pallidus and the subthalamic nucleus (STN) (Limousin et al., 1995). This structure, in addition to its role in motor control, has been shown to be involved in the development of non motor diseases such as obsessive compulsive disorders (Mallet et al., 2002). In these pathologies, it is believed that a non motor portion of the STN may receive associative and limbic information from the associative and limbic portions of the external globus pallidus. It is thus increasingly important to be able to localize with a high degree of precision not only the STN and the other nuclei of the basal ganglia, but also the topography of their functional subdivision into sensorimotor, associative and limbic territories. This subdivision, well identified in the monkey (François et al., 1994; Karachi et al., 2005; Parent, 1990), has also been established in

* Corresponding author. INSERM U679, Hôpital de la Salpêtrière, 47, boulevard de l'Hôpital, 75013, Paris, France. Fax: +33 1 45 82 88 93.

E-mail address: yelnik@ccr.jussieu.fr (J. Yelnik).

Available online on ScienceDirect (www.sciencedirect.com).

the human brain based on calbindin immunoreactivity (Karachi et al., 2002).

At the present time, magnetic resonance imaging (MRI) is certainly the most powerful imaging technique to demonstrate brain anatomy *in vivo*. Clinical brain MRI can produce 3D volumes with spatial resolution of the order of 1 mm³ or less with 1.5 T instruments. Different MRI sequences can produce different types of images, with varying contrasts optimized for depiction of different brain pathologies or normal structures. However, the spatial resolution of MRI may not be sufficient for precise imaging of small structures. Also, many deep brain structures do not exhibit detectable contrast and thus remain poorly visible or invisible at anatomical MRI. Finally, a subdivision of these structures based on functional data, which is needed for refining topographic targeting, is not available with anatomical MRI.

These are the main reasons why many DBS centers have resorted to using histological atlases. A crucial issue of this strategy is to adapt the atlas to the particular anatomy of each patient's brain. Histological atlases are most commonly employed in printed form (Mai et al., 1997; Morel et al., 1997; Schaltenbrand and Wahren, 1977) and, therefore, have to be compared and reconciled mentally with the MRI of each individual patient by the atlas user. Previously, one of the authors developed a method in which a digitized version of an atlas (Schaltenbrand and Wahren, 1977) is linearly and interactively coregistered with the patient MRI (Yelnik et al., 2000, 2003), a technique similar to that applied to an atlas of the thalamus (Morel et al., 1997; Niemann et al., 2000). However, these atlases

have two important limitations: they have a low 3D coherency and they do not include functional information.

We have thus decided to construct a new histological atlas according to the following strategy. First a postmortem specimen was obtained which was subjected to MRI scanning prior to extraction of the brain from the skull. This MRI represents the core data set that was subsequently used for the coregistration of atlas data and their deformation to conform on the MRI of living patients. Histological analysis was centered on the basal ganglia structures and comprised standard cytoarchitectonic delineation plus an immunohistochemical identification of functional subdivisions (Karachi et al., 2002). Contour tracing was optimized through multimodal and 3D validation to obtain anatomically relevant 3D surfaces.

Preliminary steps of this study have been published in conference proceedings (Bardinet et al., 2002a,b; Ourselin et al., 2001). The aim of this paper is to describe the atlas construction. The registration process of the atlas on 3D MRI of living patients is shortly illustrated in this paper while its complete description and evaluation on a retrospective series of patients will be presented and discussed in a forthcoming paper.

Material and methods

The goal of this work was to construct a three-dimensional atlas of the human basal ganglia which would have a histological degree of anatomical definition and which would comprise MRI data of the same specimen. In addition, functional subdivisions of the basal

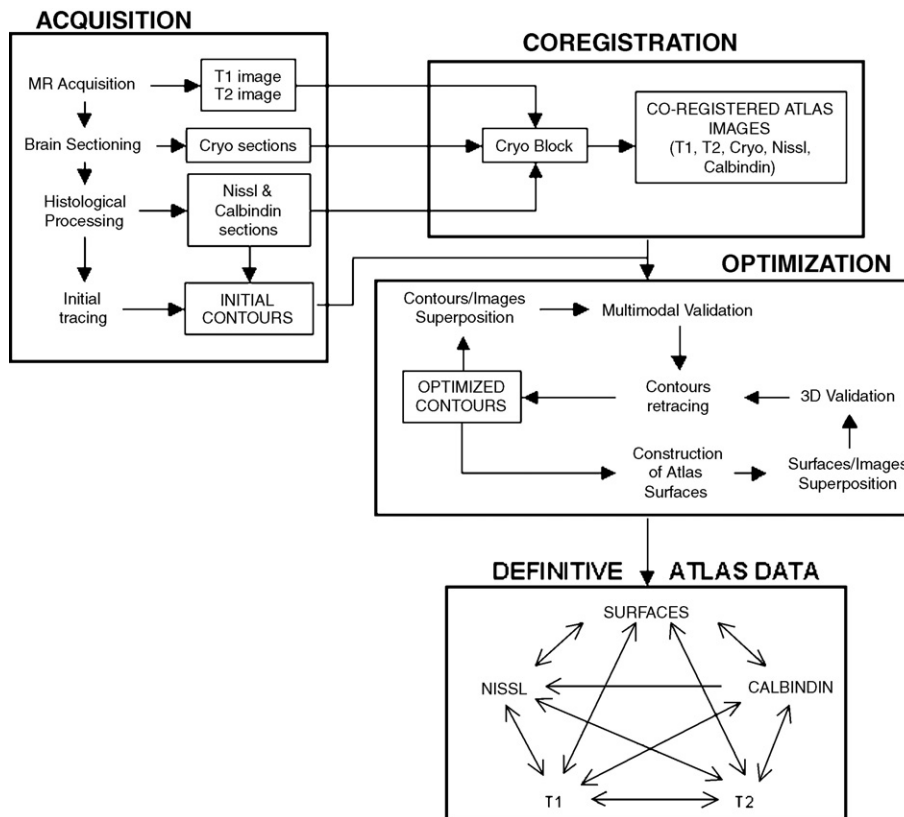


Fig. 1. Flowchart of the successive steps of atlas construction: acquisition, coregistration, optimization. This last step is conducted through two loop circuits: one loop which begins by superposition of atlas contours and atlas images allows multimodal optimization, another loop which begins by superposition of atlas images and atlas surfaces allows 3D validation of the contours. Data (in lower case letters) and results (in upper case letters) are boxed while actions are not boxed. All the definitive atlas data can be fused with each other.

ganglia should also be available in the atlas. The successive steps of the construction of the atlas, comprising acquisition, coregistration and optimization of the atlas data, are presented in Fig. 1.

Brain material

Eight brains coming from bodies donated to the Department of Anatomy, Paris V University, were selected on the following criteria: age less than 70 years, postmortem delay less than 48 h, absence of neurological or psychiatric diseases, absence of vascular or neurosurgical pathology, absence of intensive care before death. All specimens were handled in full conformance with institutional human tissue policies. The brain specimens were used to test and optimize the different steps of the processing (MRI, extraction, tissue fixation, and histological processing). The brain with the best quality of tissue imaging and fixation was selected for atlas construction. It came from a 63-year-old man who died of cardiac arrhythmia associated with non obstructive cardiomyopathy. No neurological disease was known. The MRI acquisition was made 35 h after death. The brain was taken from the skull and fixed in formalin 38 h after death.

Magnetic resonance imaging

T1- and T2-weighted sequences similar to those used for deep brain stimulation of parkinsonian patients (Bejjani et al., 2000; Dormont et al., 1997) were performed before extraction of the brain from the skull (Fig. 2). The T1 sequence was a 3D stereotactic acquisition which consisted of 124 contiguous 1.3-mm-thick slices (3D IR-FSPGR, TR=11 ms, TE=2 ms, TI=600 ms, flip angle=10°,

NEX=1, voxel size 0.9375×0.9375 mm). The T2 sequence consisted of two T2-weighted spin-echo acquisitions (TR=2200 ms, TE=90 ms, NEX=1). Each acquisition consisted of 2-mm contiguous slices. The two acquisitions were interleaved by 1 mm from each other, to obtain a series of 1-mm contiguous slices by interpolation.

Brain processing

The brain was extracted and separated into two hemispheres that were left in formalin solution (PFA 4% and picric acid 10%) for 24 h. Each hemisphere was placed in a Plexiglas box, allowing the anterior (AC) and posterior (PC) commissural points to be visualized and the hemisphere to be oriented parallel to the AC–PC line (Fig. 2). The frontal pole was removed with a cut perpendicular to the AC–PC line and a trace tracks of 2 mm in diameter were made parallel to the AC–PC line by introducing fiducial markers (metallic tubes, external diameter 3 mm, wall thickness 0.5 mm) in the hemisphere parallel to the AC–PC line and 3 cm from the midsagittal plane. Two tubes were introduced, at the AC–PC level and 3 cm more dorsally (Fig. 2), and then removed. The occipital pole was then removed and the remaining part of the left hemisphere cut into four 1.5-cm-thick blocks oriented in the frontal plane perpendicular to the AC–PC line.

Each block was post-fixed in a fresh formalin solution for 8 days at 6°C. The superior and inferior parts of the cortex were cut perpendicular to the midsagittal plane (Fig. 3) to obtain a block centered on the basal ganglia which did not exceed the dimensions of the cover glass (7×9 cm²) under which individual sections were to be mounted (Fig. 3). Blocks were then cut into 70-μm-thick

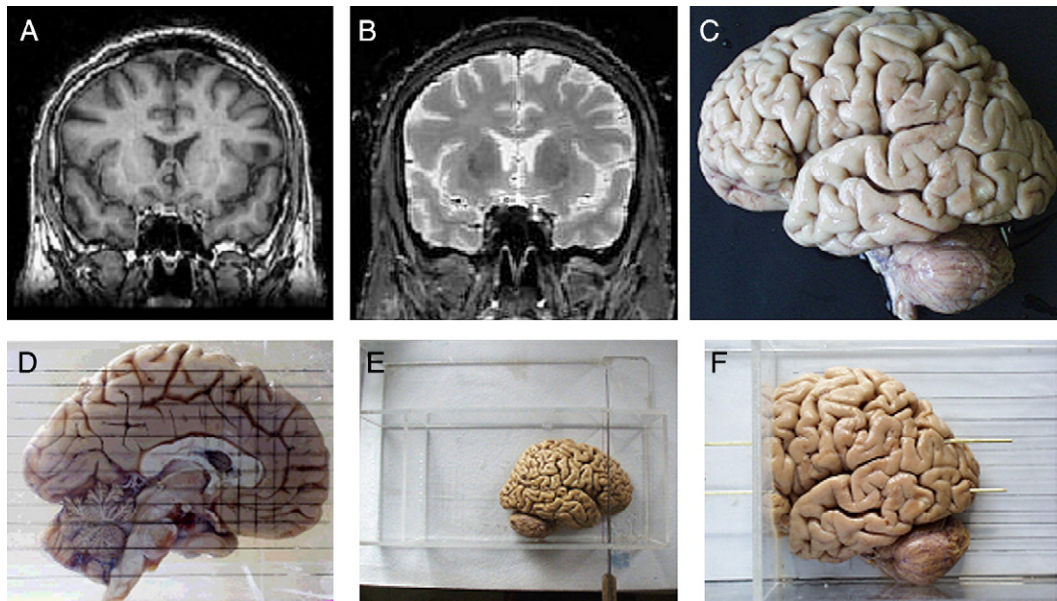


Fig. 2. Magnetic resonance imaging of the atlas specimen obtained before extraction of the brain from the skull. T1-weighted (A) and T2-weighted (B) sequences similar to those used for parkinsonian patients in the Salpêtrière group were applied. Note that the caudate nucleus and putamen are clearly identifiable and that the size of the lateral ventricles does not differ from that observed in living patients. Lateral view (C) and medial view (D) of the left hemisphere after extraction of the atlas brain from the skull. The hemisphere is laid down in the Plexiglas box so that the anterior and posterior commissural points are aligned with the lines traced on the bottom of the box. (E) A view of the Plexiglas box with the right hemisphere positioned parallel to the intercommissural line. A knife is introduced in two slits oriented perpendicular to the lines traced on the bottom of the box, which enables to cut the frontal pole perpendicular to this line. (F) Two metallic tubes are introduced parallel to the intercommissural line by using series of holes which have been made in the two walls of the Plexiglas box. These two walls are parallel to each other and perpendicular to the intercommissural line in such a way that each tube is firmly guided in the expected direction.

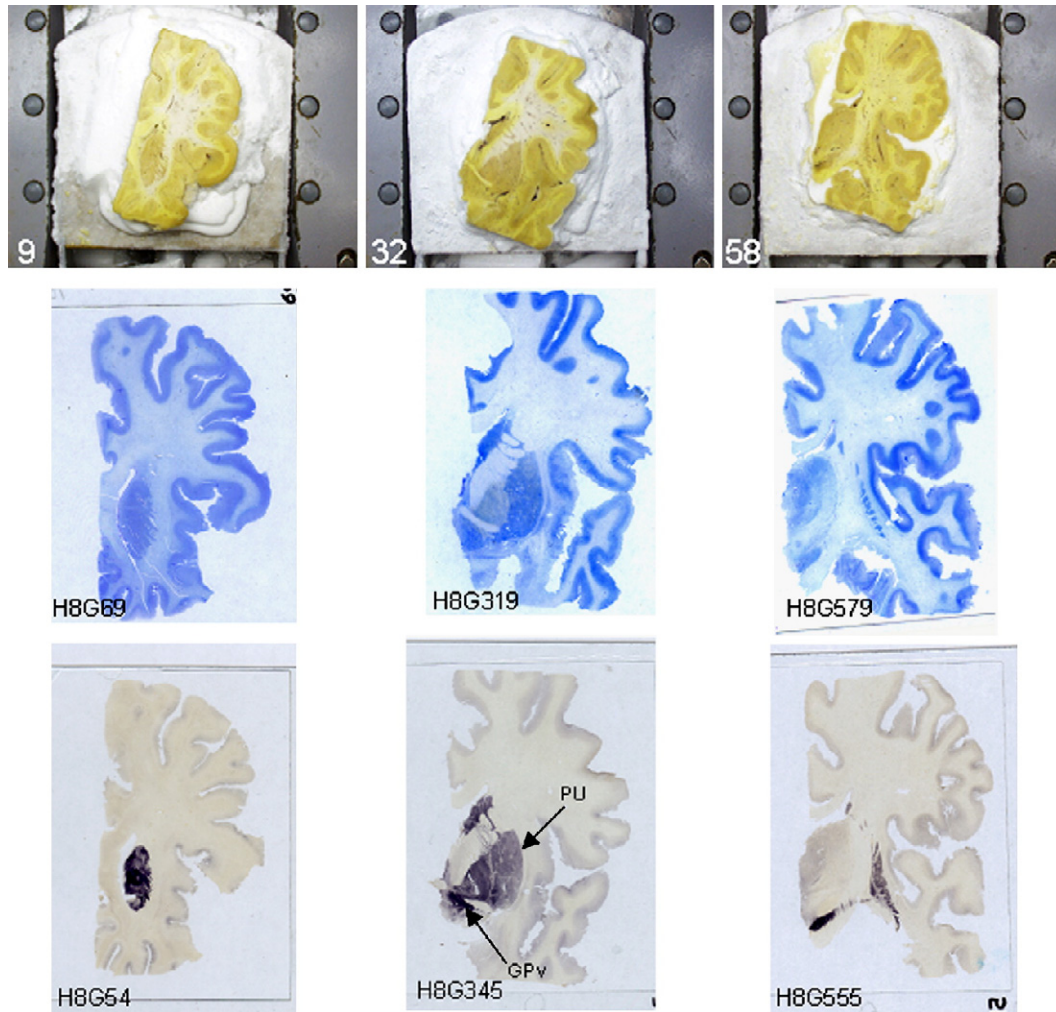


Fig. 3. Top row: Photographs taken during the process of cryosectioning. The block is embedded in carbonic ice on the stage of the microtome which is seen from the top. The three rivets seen on each side of the stage were used to align the successive pictures and reconstruct a 3D cryo block. The numeric camera was fixed on a metallic support at 60 cm from the stage. The microtome and the support were both screwed onto a laboratory board. Note that the lateral ventricle is not visible in level 9 while it was present at the same level in the MRI of Fig. 2. Middle row: Three examples of Nissl-stained sections from the left hemisphere of brain H8 from rostral level (H8G69) to caudal level (H8G579). Bottom row: Three examples of calbindin immunostained sections at similar rostrocaudal levels. Regions which strongly express calbindin are stained in brown. Note that the putamen (PU in section H8G345) is weakly stained while the subcommissural pallidum (GPv in the same section) is strongly stained. Each section is mounted between glass and cover glass ($9 \times 11 \text{ cm}^2$ and $7 \times 9 \text{ cm}^2$). (For interpretation of the references to colour in this figure legend, the reader is referred to the web version of this article.)

frontal sections on a freezing microtome (Tetrandor, Richert-Jung, Heidelberg). Photographs of the frozen blocks were taken every ten sections. The camera (Olympus Camedia C-1400 XL) was mounted on the laboratory board at a fixed distance from the microtome ensuring a constant focal distance and a field of view which included the six rivets of the microtome (Fig. 3). The 800 sections obtained were collected serially into numbered boxes. Each section was thus perpendicular to the AC–PC axis and located precisely along the anteroposterior axis of the brain. One series of sections (every tenth section, i.e. every 0.7 mm, numbered from 9, 19, 29) was Nissl-stained with cresyl violet while another series numbered from 14, 24, 34 was selected for immunostaining for calbindin (Fig. 3). An adjacent section was selected instead of the regular one when the staining of this latter was not satisfactory. Freezing of the blocks resulted in a distortion of their surfaces, the sectioning of which produced incomplete sections. In order to

compensate for this distortion, the number of incomplete sections was noted during sectioning for subsequent replacement by interpolation.

Calbindin immunohistochemistry

Sections were rinsed several times in 0.05 Tris buffer saline (TBS) pH 7.4 and permeabilized in TBS containing 0.25% Triton X-100 and gelatin (0.2%). Sections were incubated in a monoclonal antiserum raised against calbindin (Sigma, St Louis, MO) diluted to 1/1000 for 48 h at room temperature. They were then rinsed in TBS and incubated in secondary biotinylated antibody (goat anti-mouse, Amersham) at a 1/250 dilution in buffer for 2 h and then in peroxidase bound to streptavidin (1/500, Amersham). The peroxidase bound to calbindin was revealed with 3-3'-diaminobenzidine dihydrochloride (DAB, Sigma) (0.05%), 0.2% hydrogen peroxide

and nickel ammonium sulfate (0.2%). The reaction was stopped by repeated washes in TBS. If a section exhibited a too weak or too intense labeling, an adjacent section (numbered 5, 15, 25, etc., or rarely 6, 16, 26, etc.) was selected and immunostained. The position of this new section in the anteroposterior sequence was taken into account in further processing.

Software tools

Three different software tools were used in this study. A Three-dimensional Tracing Software application (TTS) was developed by the INSERM group for the purpose of digitization and processing of serial cerebral contours. The TTS provides various tools for contours visualization and interactive modification (see Appendix A for details). The Yav++ software package was developed by the Epidaure group at INRIA (Delingette et al., 2001). Principal features of Yav++ include comparison and fusion of 3D images in multiplanar viewers as well as a 3D camera allowing visualization of serial contours, 3D surfaces and 3D images in the same image (see Appendix B for details). The BALADIN software, an automatic image registration algorithm, was also developed by the Epidaure group at INRIA (Ourselin et al., 2000). It allows registration of 2D or 3D images through an intensity-based robust block-matching approach (technical details in Appendix C).

Atlas data acquisition

Nissl-stained and immunostained sections were observed under the $\times 2.5$ objective of a Leitz Orthoplan microscope. Higher power objectives ($\times 16$ or $\times 40$) were also used to examine cytoarchitectural details and to determine the exact tracing of cerebral structures. Contours of each cerebral structure and of regions of different intensities of calbindin labeling were traced under the microscope with the aid of an XY plotter connected to the stage of the microscope as was done previously in the monkey (François et al., 1996). Drawings were performed at $\times 10$ magnification i.e. 100 μm for 1 mm. The initial tracing of the calbindin-labeled regions has previously been published (Karachi et al., 2002). The contours were then digitized using the TTS and a Summa sketch III (SummaGraphic) XY digitizer. The reference axes determining the space in which the initial contours were traced was determined based on the tracks that the fiducial markers left on each section (Fig. 4). The dorsoventral axis was traced parallel to a line passing through the two tracks and 3 cm medial to them. The mediolateral axis was traced perpendicular to the dorsoventral axis and passing through the inferior track. The intersection between the two axes was the zero point of the section. Each contour was then transformed into a series of x and y coordinates measured with reference to the mediolateral and dorsoventral axes. The z coordinate was given for each section by its position along the AC–PC axis, taking the PC point as the origin of the system of axes. Arbitrarily, positions anterior, superior and left to the origin were defined as positive. For the incomplete histological sections corresponding to the surfaces of each block, missing contours were traced by interpolation with adjacent complete sections.

Atlas data coregistration

The atlas image data consisted of five different series: T1- and T2-weighted MRI acquisitions, photographs taken during the cryosectioning of the brain, Nissl and calbindin 2D sections. Careful

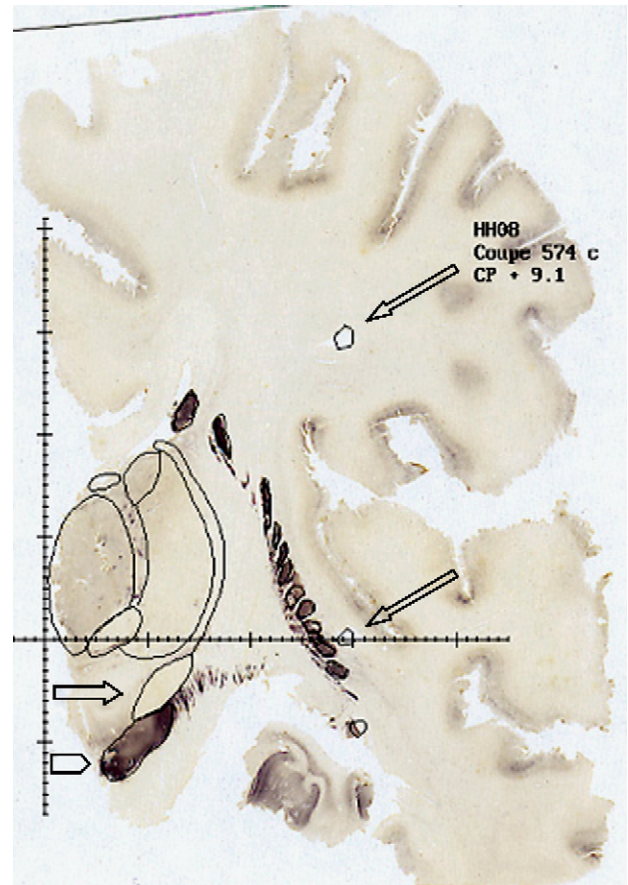


Fig. 4. Example of the initial tracing of cerebral contours in a calbindin immunostained section. The two oblique arrows indicate the tracks that the horizontal metallic tubes left in each section. The inferior track indicated the horizontal mediolateral axis passing through the level of the posterior commissure, the superior track was 3 cm more dorsal. The two tracks were 3 cm lateral to the midsagittal plane. The open arrows points the subthalamic nucleus, the arrowhead points the substantia nigra.

analysis of the protocol of data acquisition allowed to choose a method of coregistration specifically adapted to the different types of distortion affecting the various types of data. Indeed, brain extraction, fixation and freezing induced mostly smooth 3D deformations, whereas sectioning followed by histological processing induced variable non-linear 2D distortions. Therefore, coregistration was performed in two steps: first, a 3D block was reconstructed from the 2D histological sections (in order to provide accurate and coherent alignment of the contours traced on the histological sections), second, the 3D block was registered with the corresponding MRI data. Two points asked for special attention, namely the 3D integrity of the reconstructed volume and the preservation of the anatomical information provided by the histological sections. To cope with the first one, we used cryo sections as an intermediate dataset, because the microtome rivets included in the photographs served as fiducials for the alignment of these sections. This provided a coherent 3D block, which served as a reference both for building an histological 3D block and for registering with the MRI data. Histological information was preserved through the application of such a registration scheme.

First, the reconstruction of a 3D cryo image was performed (Fig. 5). Photographs taken during cryosectioning of the brain

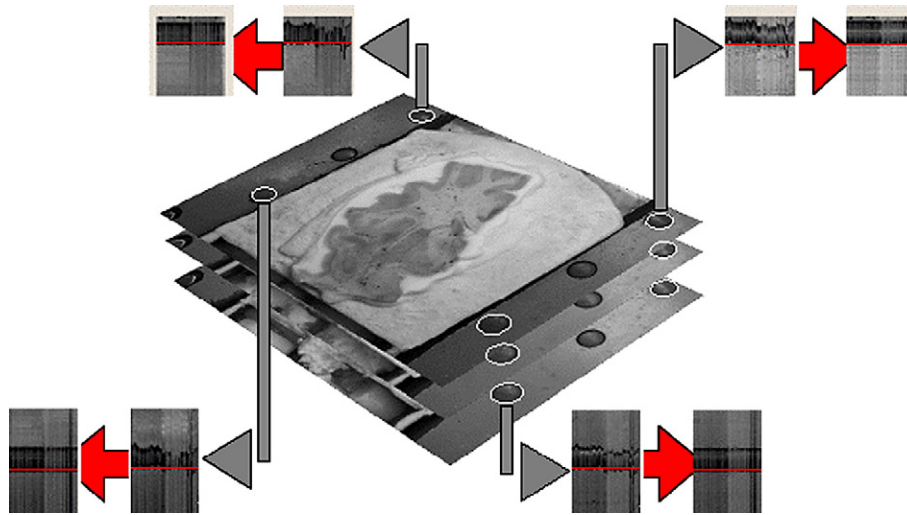


Fig. 5. Atlas data coregistration (I): alignment of cryo sections. Original cryo sections have been digitized and stacked (center of figure); rivets of the cryomicrotome have been automatically extracted; slice-to-slice 2D rigid registrations of the resulting binary images yielded aligned cryo sections (the four snapshots focus on stacks of rivets before and after rigid alignment).

(referred to as cryo sections) were aligned into 3D cryo blocks (one cryo block for each 1.5-cm-thick block – see Brain processing) following three steps: (a) the 6 rivets of the freezing microtome, included in the field of view for every section (Fig. 3), were extracted automatically using an elementary image processing pipeline (threshold selection, mathematical morphology operators and connected components extraction); (b) in the resulting series, every binary image was rigidly registered to its immediate neighbor by means of an image-based registration algorithm based on the Iterative Closest Points matching technique (ICP) (Besl and McKay, 1992) with the rivets used as fiducial markers; (c) once every pair of consecutive images was registered, composition of the corresponding transformations applied to the original cryo sections yielded a 3D cryo block (for each cryo block, the first section was used as reference). Then, inter cryo block registration was performed by rigidly aligning the last section of a cryo block with the first section of the next cryo block, using the BALADIN software (fiducial markers could not be used because of the block change on the cryomicrotome). Finally, differences in signal intensity in the cryo sections were corrected by applying an intensity compensation algorithm (Malandain and Bardinet, 2003). This yielded the whole 3D cryo block.

Second, the histological slices were registered with the 2D cryo images (Fig. 6), yielding both a reconstructed 3D histological image, and its coregistration with the 3D cryo image. Nissl and calbindin sections were scanned using high resolution settings (500 ppi) and background was automatically removed using low-level image processing techniques (threshold and mathematical morphology operators, and connected components extraction). Each histological section was then separately registered onto the corresponding level of the cryo block¹ by means of the following five steps: (a) each

section was rigidly registered onto its corresponding cryo section; (b) the composition of the corresponding transformations was applied to the original histological sections, which were stacked, yielding a first 3D histological block; (c) a 3D region of interest centered on the basal ganglia (limited by the corpus callosum along the anteroposterior axis, and dorsally, by the cerebral peduncle ventrally and by the insula laterally) was extracted from the histological and cryo blocks, using the Yav++ software, and the two blocks were unstacked, yielding histological and cryo sections centered on the basal ganglia; (d) each cropped histological section was registered onto its corresponding cryo section (following a hierarchical strategy using rigid, scale and affine transformations); (e) composition of the last transformations obtained was applied to the histological sections yielding the 3D histological image. All these registrations were performed with the BALADIN software.

Third the coregistration of the 3D cryo image and the T1-weighted MRI was performed. The cryo image was selected for this step because it was less affected by distortion during processing than the histological 3D reconstructed image. The T1-weighted MRI was selected because it demonstrates less distortion (Menuel et al., 2005) and its contrast is more similar to sectioned brain tissue. Coregistration was performed following five steps: (a) on the T1-weighted MRI, the brain was separated into two hemispheres, by automated detection of the midsagittal plane (Prima et al., 2002) and only the left hemisphere was further considered; (b) global rigid registration was performed between the MRI and cryo block images using the BALADIN software; (c) a region of interest centred on the basal ganglia was extracted from the two rigidly registered images; (d) local hierarchical registration (rigid, homothetic and affine) was performed between the two regions of interest.

Finally, the coregistration of the T1- and T2-weighted MRIs was performed using global hierarchical registration including rigid, homothetic and affine steps with the BALADIN software.

At this stage, all atlas image data were coregistered, meaning all data were defined in a common reference frame. The transformations retained for this coregistration were determined at this stage of atlas construction and considered as definitive. The initial 2D

¹ As photographs of the frozen block were taken every ten sections (70 μm thick), and as histology was processed every five sections (one Nissl and one calbindin alternatively), each photograph corresponded to both a Nissl and a calbindin section, each being located at 350 μm distance.

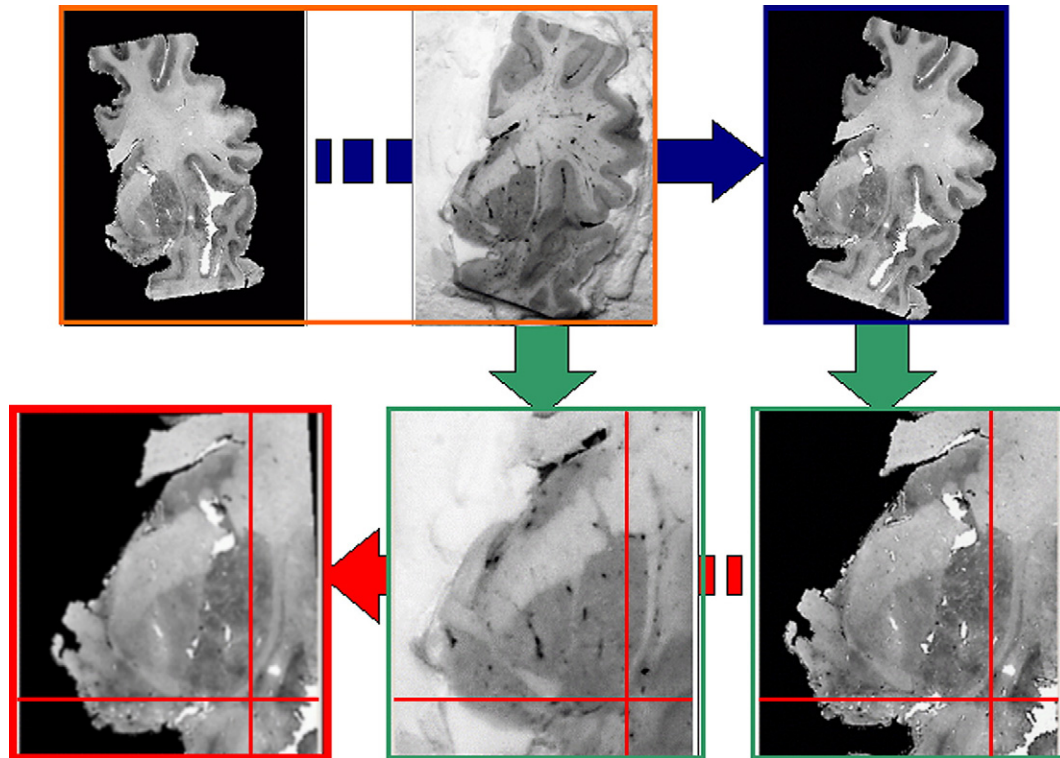


Fig. 6. Atlas data coregistration (II): coregistration of histological and cryo sections. Histological sections have been digitized; each histological section has been independently registered onto its corresponding cryo section, following a three-step procedure (from top left, clockwise): starting with the original histological and cryo sections (top line, left), the histological section was first registered rigidly (top line, right), then a region of interest centered around the basal ganglia was automatically extracted on both sections (bottom line, right), and the matching was refined by means of a local affine transformation (bottom line, left). Bottom line: the red axes point out the same pixel in the three slices, allowing to visually assess both the quality of the final registration and the slight improvement provided by the local registration step. (For interpretation of the references to colour in this figure legend, the reader is referred to the web version of this article.)

contours traced on the histological sections could be transferred on every 3D image or reconstruction.

Atlas data optimization

Construction of 3D meshes from these serial 2D contours followed. To obtain surfaces which could be sliced in any direction, an optimization including multimodal and 3D validation of the initial contours was necessary. The methods used for these different steps are now detailed.

The adequacy of the initial tracing of each contour of each cerebral region with each modality (T1, T2, cryo, Nissl, calbindin) was systematically verified and corrected when necessary. This was done by an anatomist (JY), based on current anatomical knowledge. Depending on the cerebral structure considered, one of the five modalities could be given priority and employed as the reference standard (Fig. 7). The retracing was then superimposed on the atlas images and subjected to multimodal validation again (Fig. 1). The 3D coherency of successive contours was verified by slicing the contours of one or two structures in the sagittal plane (Fig. 8) and identifying irregularities which were not valid anatomically. 3D adjustment was accomplished by retracing the corresponding contours in the TTS environment (Fig. 8) (see also Appendix A). Quantitatively, two different levels of correction were made between initial and optimized tracings (Fig. 9). The first correction level was a smoothing consisting of sub-millimetric adjustments (open arrows

in Fig. 9) to make the 3D contours smooth, as illustrated in Fig. 8. The second correction level was an anatomical retracing that was necessary when larger (1–3 mm) 3D inconsistencies appeared (black arrows in Fig. 9). Such errors, due to uncertainties of the initial tracing or residual errors of the coregistration, were corrected by modifying the tracing in several adjacent sections. A 3D rotation of all the dimensions of space was also used during the optimization process to check the 3D coherency of the contours (Fig. 8). This optimization procedure is further commented upon in the Discussion.

Atlas surfaces were constructed from these optimized atlas contours using shape-based interpolation (Herman et al., 1992). Another 3D validation was then performed using the Yav++ application with which atlas surfaces can be fused with the five 3D block modalities and visualized simultaneously in the axial and sagittal planes (see Appendix B). This provided the most powerful tool to verify the 3D consistency of the atlas surfaces. If an unexpected tracing appeared in any plane of section, the multimodal and 3D validity of the tracing was verified and modified if necessary.

In summary, optimized atlas surfaces were obtained by an iterative combination of contours validation and construction of 3D surfaces performed through two intricate loops (Fig. 1). The first loop, centered on the multimodal validation, allowed us to assign priority as the reference standard to the most reliable modality for each cerebral structure. The second loop, based on the construction of atlas surfaces and their superposition with the 3D atlas images

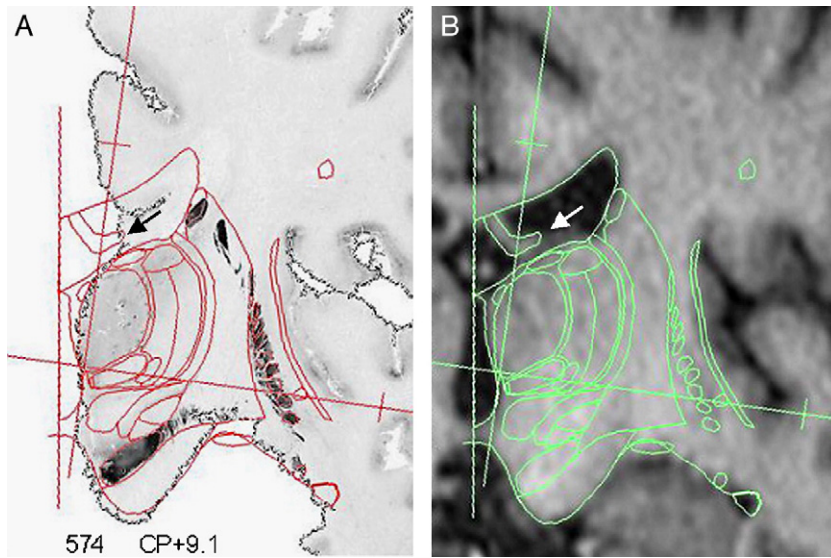


Fig. 7. Tracing of cerebral contours in the section 574 after multimodal optimization. The contours are superimposed with the corresponding calbindin section (A) and T1 MRI section (B). Note that the fornix (arrows), which was not visible in the calbindin section, could be delineated in the T1 MRI section.

(MRI, Nissl, and calbindin), permitted the verification of the 3D consistency of the surfaces and their correction when irregularities were noted. Contours were considered as definitely optimized when the best compromise was obtained between histological truth and 3D anatomical consistency.

Results

Atlas data acquisition

The MRI obtained before extraction of the brain from the skull (Fig. 2) was very similar to the images obtained with the same parameters for living patients. The only noticeable difference was a slight reduction of contrast between grey and white matter. The longest distance between the frontal and occipital poles as measured after extraction of the brain (Fig. 2) was 17.2 cm. The AC–PC distance determined on the medial aspect of the left hemisphere between the posterior margin of AC and the anterior margin of PC was 23.2 mm. Sectioning of the left hemisphere after removal of the frontal and occipital poles (Fig. 2) produced four 1.5-cm-thick blocks in the region of the basal ganglia which were sectioned on a freezing microtome (Fig. 3). Two kinds of distortion occurred at this stage. First, interhemispheric sectioning resulted in a leakage of cerebral fluid and a noticeable collapse of the ventricle, which can be seen by comparing an MRI section (Fig. 2) with the cryo image of the same level (9 in Fig. 3). Second, freezing of the blocks for cryosectioning resulted in a distortion of the surface of the blocks, the center of a block being generally thinner than its periphery. As a consequence, the first histological sections corresponding to the surfaces of each block were incomplete. The number of these incomplete sections was noted during sectioning.

The first block yielded 36 reference sections including 17 Nissl and 18 calbindin sections numbered 14 to 186 and contained the anterior poles of the caudate nucleus and putamen. Examples of Nissl-stained and calbindin immunostained sections are given in Fig. 3. The space between block 1 and block 2 was estimated to be approximately four reference sections (189, 194, 199, and 204). The inferred gap was considered to be occupied by four virtual sections, a

distance of 1.75 mm, for which the cerebral contours were constructed by interpolation between sections 186 and 210. This interpolation procedure was followed for each of the three interblock gaps. Block 2 yielded 38 sections (19 Nissl and 19 calbindin) numbered from 210 to 395. The anterior commissure was in the mid part of this block and the anterior pole of the thalamus started in its posterior part. The space between blocks 2 and 3 was estimated to be approximately 6 sections (399, 404, 409, 414, 419, and 424), a distance of 2.5 mm. Block 3 yielded 35 sections (18 Nissl and 17 calbindin) numbered from 430 to 599 and contained the largest part of the thalamus and subthalamus and the anterior pole of the substantia nigra. The space between blocks 3 and 4 was estimated to be approximately 6 sections (604, 609, 614, 619, 624, and 629), a distance of 2.5 mm. Block 4 yielded 28 sections (18 Nissl and 10 calbindin). The 18 Nissl sections (numbered from 639 to 809) and the 10 calbindin sections (numbered from 635 to 725) contained the posterior part of the caudate nucleus and substantia nigra. Seven additional sections numbered from 734 to 794 were interpolated from the adjacent couples of Nissl sections. Contours of the basal ganglia structures, grey nuclei, white matter regions and functional subdivisions, were traced in the 160 sections which constituted the atlas.

Atlas data coregistration

The first step of atlas data coregistration was the construction of the cryo block by using the rivets of the microtome as described in Material and methods. Visual inspection revealed satisfactory alignment of the rivets (Fig. 5). Results of the inter cryo block registrations were carefully checked by the anatomist (JY) using the Yav++ software in order to validate the consistency of the entire resulting 3D cryo block which was further used for coregistration of histological sections and postmortem MRI data. The results of the registration between individual histological 2D sections and corresponding cryo sections were considered to be of good quality (Fig. 6). Then 3D histological blocks were constructed by composition of all transformations. Results were considered to be of very good quality as exemplified by the bridges of grey matter

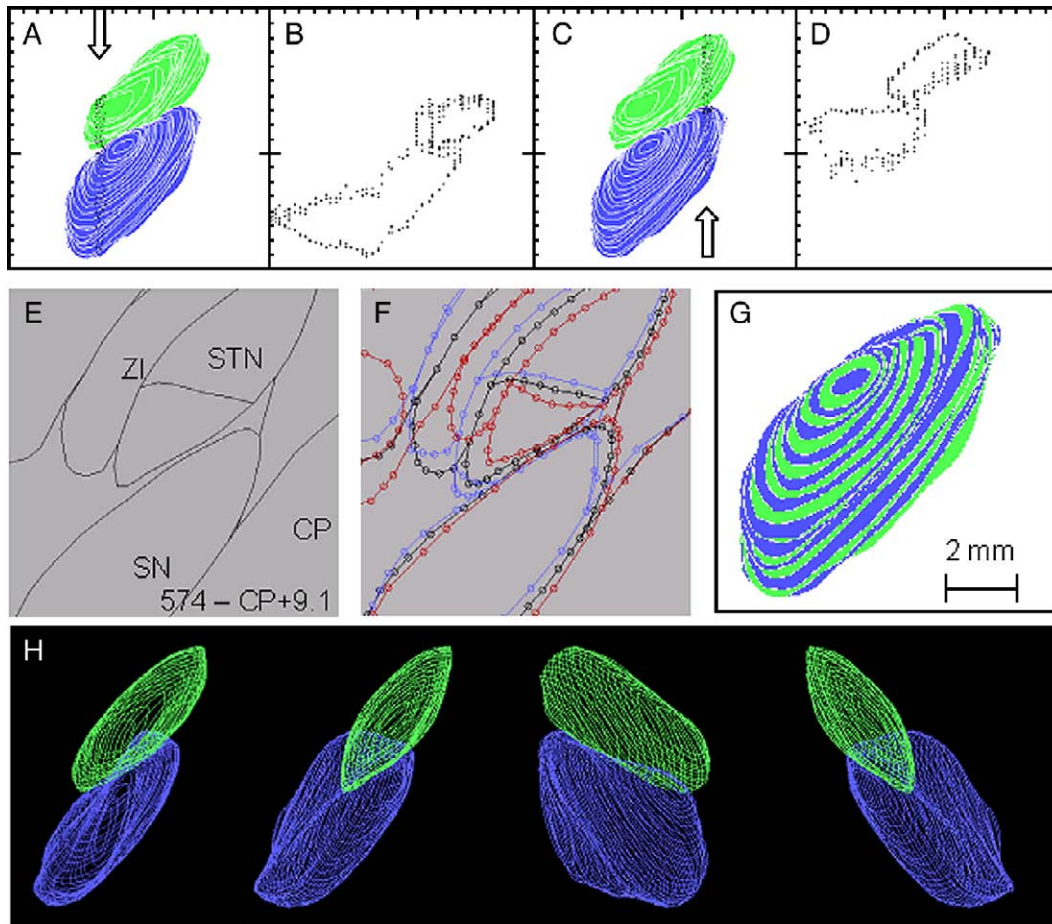


Fig. 8. Three-dimensional optimization of contour tracing. (A) Anterior view of the successive contours of the subthalamic nucleus (green) and substantia nigra (blue). The arrow indicates the position of a sagittal slice that was selected and the corresponding points of the two contours. (B) The same points are displayed in a sagittal plane. (C) Another more lateral slice is shown with the corresponding sagittal view in (D). The slice thickness was adjusted at 0.7 mm. (E) Detail of contours traced in section 574 (vector mode in the TTS software application, zoom on subthalamic region). (CP=cerebral peduncle, SN=substantia nigra, STN=subthalamic nucleus, ZI=zona incerta). (F) The same section is represented with the digitized point indicated as small circles (point mode in TTS). The same contours in the adjacent calbindin-stained sections are shown in blue (section 564) and red (section 584). Note that the spacing between adjacent contours is smaller for the substantia nigra than for the subthalamic nucleus and zona incerta showing that the contour of the former is almost perpendicular to the frontal plane while the contour of the two latter is much more oblique. With the computer program used, each point could be displaced using the mouse. (G) Anterior view of the successive contours of the subthalamic nucleus with those traced in calbindin and in Nissl sections colored in green and blue, respectively. The twelve most anterior contours have already been optimized which results in regularly spaced contours. Conversely, the posterior contours appear as irregularly spaced curves. Scale bar in panel G also applies to panels E and F. (H) 3D rotations of the subthalamic nucleus (green) and substantia nigra (blue) contours after 3D optimization. Note that the overall shape of the two structures is smooth whatever the angle through which it is viewed. (For interpretation of the references to colour in this figure legend, the reader is referred to the web version of this article.)

between the caudate nucleus and putamen which demonstrated a very good correspondence between the Nissl, calbindin and cryo blocks and a smooth continuity in the three dimensions (Fig. 10). These bridges are thin structures that are obliquely oriented with respect to the atlas anatomical planes. Thus, they were of particular interest in the evaluation of the goodness-of-fit of the coregistration. 3D coherency of the three modalities is also illustrated in Fig. 11 in which the continuity of cerebral structures is clearly apparent. Coregistration between the T1 MRI and the cryo block provided the final link between histology and MRI of the same brain. Coregistration of all atlas data was completed by the registration of T1 and T2 MRIs. The accuracy of the correspondence between registered T1 MRI, T2 MRI and cryo block is illustrated in Fig. 12.

The outcome of atlas data coregistration thus consisted of a set of multimodal data (cryo, Nissl, calbindin, T1, and T2) integrated in a

common frame of reference. This represented a unique tool with which contours of basal ganglia structures could be compared to each of these modalities and adjusted when necessary.

Atlas data optimization

The AC–PC length was re-measured after fusion of the histological data with the MRI acquisition and optimization of contours tracing. The distance between the centers of the commissures was 26 mm. The distance between the posterior margin of AC and the anterior margin of PC was 24.4 mm.

Registration of the histological blocks with the MRI acquisition revealed an 8° difference between the midsagittal plane (MSP) traced from histological data (Fig. 4) and the true MSP as seen on MRI data (Fig. 7B). This difference, apparently due to flattening of

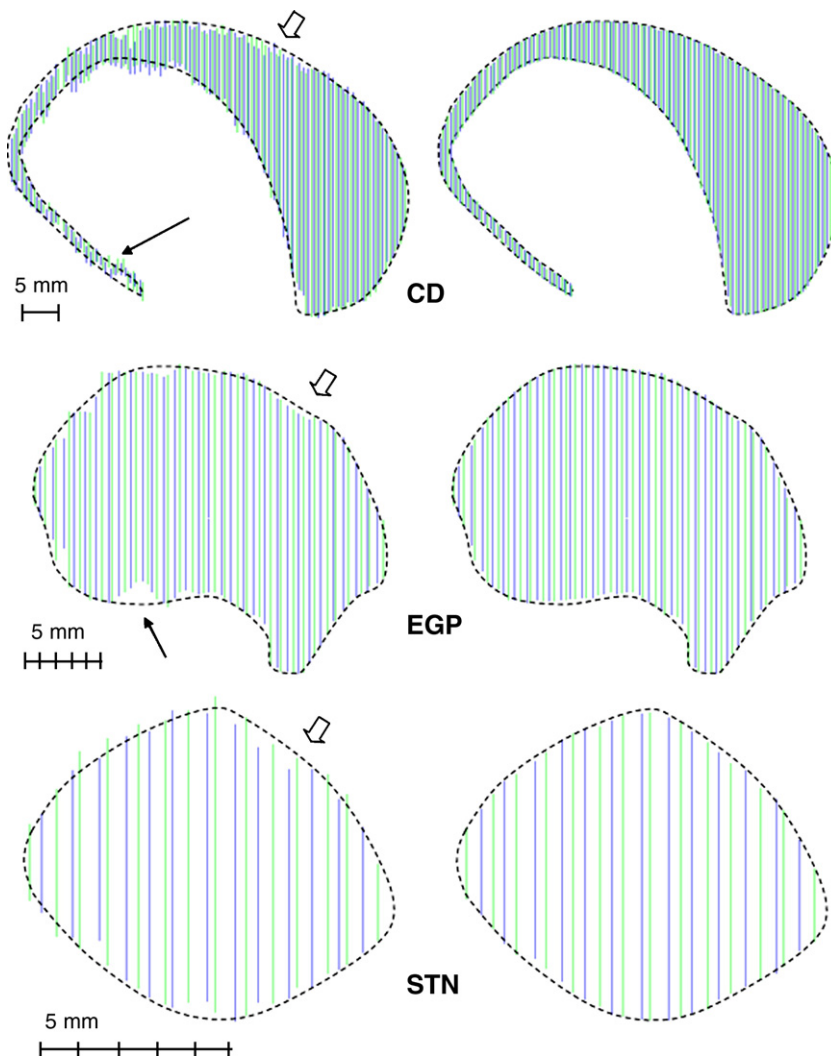


Fig. 9. Comparison between the tracing of the caudate nucleus (CD), external globus pallidus (EGP) and subthalamic nucleus (STN) before (left column) and after (right column) multimodal and 3D optimization. Each structure is seen through a 90° sagittal rotation with the tracing made in Nissl-stained and calbindin-stained sections indicated by different colors (blue and green, respectively). Open arrows show regions of sub-millimetric smoothing, black arrows show regions of supra-millimetric anatomic retracing. Spacing between successive sections can vary slightly when adjacent sections exhibiting better calbindin or Nissl staining were selected instead of the regularly spaced sections (see Material and methods). (For interpretation of the references to colour in this figure legend, the reader is referred to the web version of this article.)

the lateral ventricle resulting from cerebrospinal fluid leakage during brain extraction and interhemispheric sectioning, had no effect on surface construction as all coregistered atlas data are expressed in the 3D MRI space.

Atlas data optimization, performed for all basal ganglia contours, required different levels of adjustments. Three structures can be seen in Fig. 9 as examples. In general, optimization of the contours was conducted to obtain anatomically relevant contours in the three dimensions. 3D smoothing of contours was made primarily in the anteroposterior direction, perpendicular to the frontal plane of acquisition, to obtain isotropic regularity of the structures. Adjustment was obtained by very small (less than 0.1 mm, almost invisible in Fig. 9) displacements of individual points. Irregularities were not smoothed when anatomical structures were known to be irregular such as the bridges of grey substance which link the caudate nucleus to the putamen. Contours of the subthalamic region (STN, substantia nigra, and red nucleus)

required only fine sub-millimetric smoothing while other contours such as the caudate nucleus and globus pallidus required 3D smoothing as well as some anatomical (up to 2 mm) retracing (Fig. 9). The quantitative effect of the optimization procedure was estimated by comparing the initial and final volumes of the main basal ganglia structures: caudate nucleus +2.8%, putamen -0.15%, external globus pallidus +4.6%, internal globus pallidus +5.9%, substantia nigra +0.6%, STN +0.15%.

Definitive atlas data

Basal ganglia grey nuclei

The caudate nucleus, putamen, external and internal globus pallidus were initially traced from both Nissl and calbindin stained sections (Fig. 3). This tracing was optimized by comparison with the appearance of the same structures on MRI (Fig. 13).

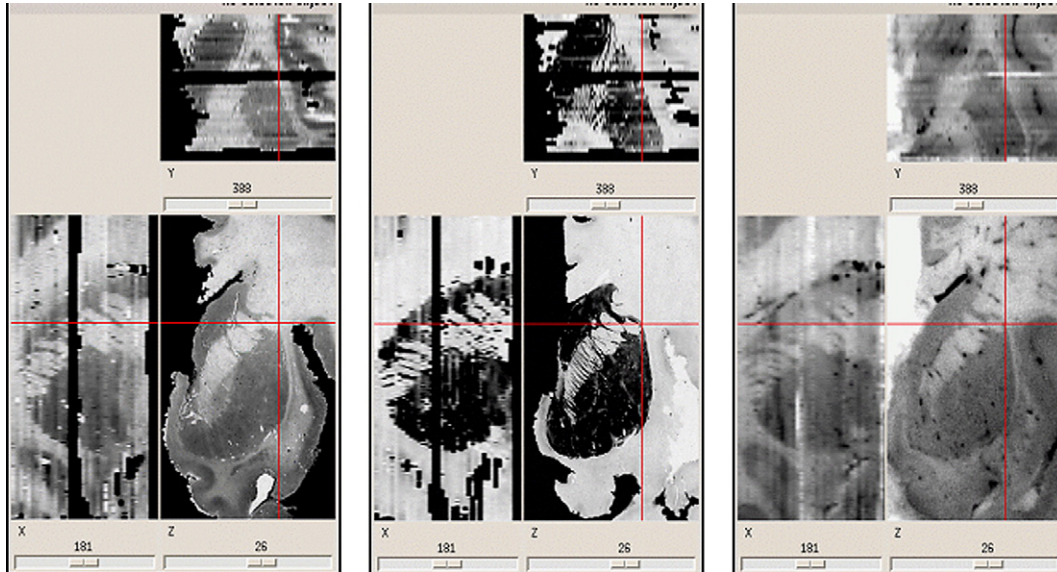


Fig. 10. Cryo sections alignment and histological to cryo section registrations yield coregistered 3D histological and cryo blocks. From left to right: Synchronized multiplanar views (sagittal, axial and frontal planes) of the Nissl, calbindin and cryo blocks, focusing on the bridges of the interna capsula. Visual inspection reveals excellent correspondence between the three blocks and smooth continuity in the sagittal and axial planes.

The contours of the STN were contained in 14 calbindin levels and 13 Nissl levels. The STN appeared as a clearly delineated zone devoid of calbindin labeling, which contrasted with the densely labeled ventrally located substantia nigra (Fig. 4). The STN was also clearly identified cytoarchitecturally in Nissl-stained sections. The 3D coherence of the STN contours was controlled on the 3D viewer which showed that contours in the sagittal and axial planes were smooth (Fig. 14) and that their relationship to the zone of hypointense signal on T2-weighted MRI was similar to that demonstrated in living human brains (Dormont et al., 2004).

The contours of the substantia nigra were traced in 22 calbindin levels and 22 Nissl levels. 19 contours were in the third block, 19 in the fourth block and 6 contours corresponding to the incomplete sections at the block surfaces were interpolated. The contours of the substantia nigra were traced together with those of the adjacent

cerebral peduncle which extended through 55 levels and which was clearly identifiable on T1 MRI. The red nucleus, medial lemniscus, caudal zona incerta and brachium conjunctivum were also traced in Nissl- and calbindin-stained sections and aligned based on T1 and T2 MRIs.

Basal ganglia functional subdivisions

The identification of the basal ganglia functional subdivisions was based on the calbindin immunostaining as described in a previous paper (Karachi et al., 2002). Starting from the 24 frontal levels analyzed in this study and from the other intermediate calbindin sections, the contours of each functional territory were interpolated in the complete series of the 160 atlas sections. This resulted in atlas surfaces corresponding to the sensorimotor, associative and limbic territories of the caudate nucleus, putamen, external globus pallidus and internal globus pallidus (Fig. 15).

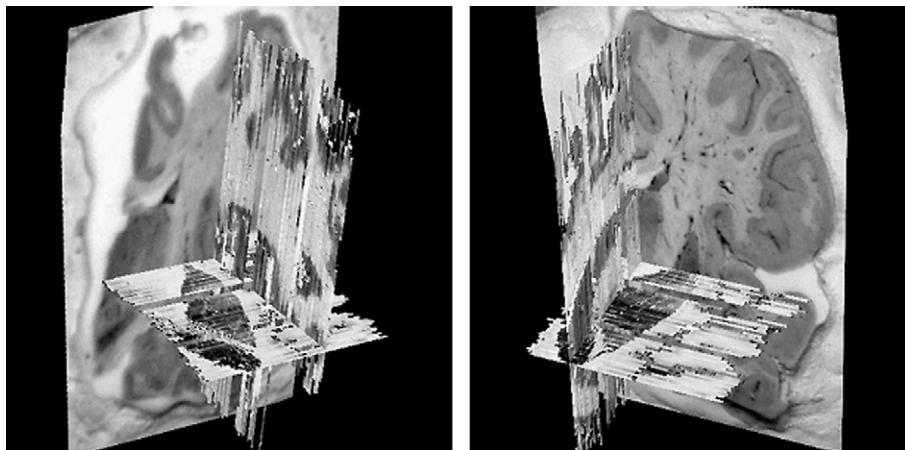


Fig. 11. Coregistration of cryo and histological sections. In this 3D view, the axial plane is a calbindin section, the sagittal plane is a Nissl section and the frontal plane is a cryo section. Note the good correspondence at the level of the caudate nucleus and putamen.

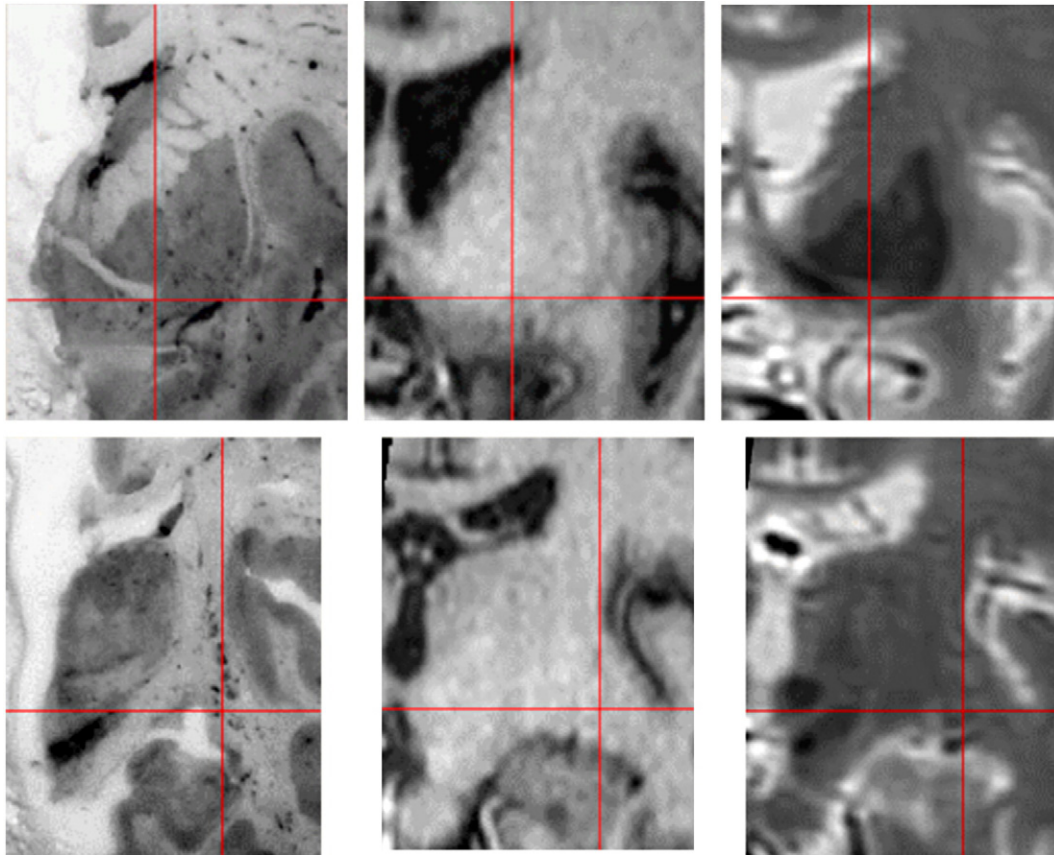


Fig. 12. Coregistration of 3D cryo block with T1- and T2-weighted MRI. In the upper row the red cross is positioned on the lateral limit of the anterior commissure. In the lower row it is positioned on the upper limit of the substantia nigra and the medial limit of the insular cortex. (For interpretation of the references to colour in this figure legend, the reader is referred to the web version of this article.)

In the STN, calbindin immunostaining could not be used because this nucleus does not contain this calcium binding protein. In order to approximate the limits of the three territories in the STN, we reasoned by homology from a cartography obtained in the monkey by axonal tracing from the external globus pallidus (Karachi et al., 2005) (Fig. 16).

Basal ganglia white matter

Axonal bundles were digitized as individual cerebral structures as they provide topographic information that can be particularly useful in a neurosurgical context (e.g. localizing the different contacts of a deep brain stimulation electrode on a patient's MRI). The internal capsule and cerebral peduncles were traced using Nissl, calbindin and MRI data and optimized in three dimensions. Particular attention was paid to the fascicles which traverse the subthalamic region and are afferent to the thalamic nuclei: medial lemniscus, brachium conjunctivum, Forel's fields H, H1 and H2 and the ansa lenticularis. Along with other cerebral regions of this atlas, these fascicles were transformed into 3D surfaces (Fig. 17) which could be sliced in any direction and provide smooth and anatomically reliable bidimensional contours in any plane of section.

Other brain structures

The contours of the ventricles, which collapsed during interhemispheric sectioning of the specimen, were traced directly on the T1 MRI. The mammillary body, fornix and anterior part of the optic tract were also traced on the T1 MRI in which they were

completely identifiable (fornix in Fig. 7). The mamillothalamic tract which interconnects the mammillary body with the anterior nucleus of the thalamus (Fig. 18) was traced in the T1-weighted MRI and the calbindin sections.

The main divisions of the thalamus were delineated in Nissl- and calbindin-stained sections. The internal medullary lamina and the perithalamic reticular nucleus were used as landmarks to subdivide the thalamus in the frontal plane and delimit the mediodorsal nucleus from the lateral thalamic nuclei (Fig. 19). The latter were subdivided into four anteroposterior subdivisions (anterior, lateral, intermediate, and posterior) which correspond to the expected regions of termination of nigral, pallidal, cerebellar and lemniscal afferents described in experimental studies (Percheron et al., 1996).

Atlas data availability

The atlas consists today of a series of digitized contours and the corresponding 3D sliceable surfaces, MRI T1 and T2 acquisitions of the same brain before extraction and histological block preparations (Nissl and calbindin). The software tools that have been developed to deform these surfaces onto the MRI of a given patient are to be published in a forthcoming paper.

Discussion

Accurate and detailed identification of the basal ganglia anatomy in a given patient is increasingly required in the clinical and cognitive neurosciences. In particular, DBS neurosurgery,

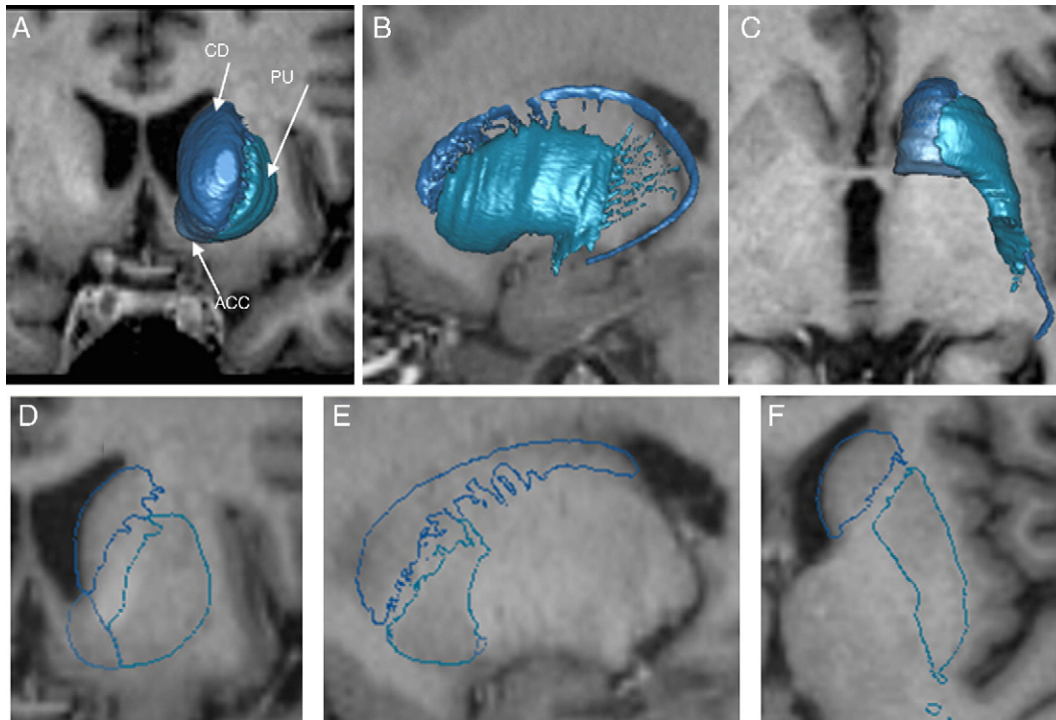


Fig. 13. Anterior (A), lateral (B) and inferior (C) views of the atlas surfaces of the caudate nucleus (CD), putamen (PU) and nucleus accumbens (ACC) created from the optimized atlas contours. Frontal (D), sagittal (E), and horizontal (F) sections of the same structures after fusion with the T1 MRI of the atlas brain allowing to verify the 3D consistency of atlas surfaces.

initially applied to tremor and Parkinson's disease, is being applied to other brain pathologies with DBS targets that have become progressively smaller as pathophysiological models are refined. Because the scale of these targets is below the spatial and/or contrast resolution of clinical practice MRI, atlas-based methods are the only way to identify all the basal ganglia nuclei. The best known atlases of the human brain comprise the hemispheres (Mai et al., 1997; Schaltenbrand and Bailey, 1959; Schaltenbrand and Wahren, 1977; Talairach et al., 1957; Talairach and Tournoux, 1988), or the brain stem and cerebellum (Afshar et al., 1978), or the thalamus (Andrew and Watkins, 1969; Morel et al., 1997; Van Buren and Borke, 1972). Some present both histology (cyto- and/or myelo-architectony) and contour tracing (Mai et al., 1997; Morel et al., 1997; Schaltenbrand and Wahren, 1977) while others propose only contour drawings (Talairach and Tournoux, 1988) or MRI with photographs of brain sections (Duvernoy, 2004).

The novel advance provided by the present digitized brain atlas is that histological data were acquired with the specific aim of obtaining consistent histology in 3D. This was obtained by selecting thin slices (70 μm) at short intervals (350 μm) and comparing the series of histological slices with the 3D MRI of the same specimen. Moreover, a functional cartography of the subdivisions that process motor, cognitive and emotional information is provided. In this regard, the present atlas differs from other published atlases. Most previous atlases have been built by tracing the contours of cerebral structures as they appear in each histological section and are validated by presenting face to face photographs of the histological sections and the corresponding tracing of cerebral contours (Mai et al., 1997; Schaltenbrand and Wahren, 1977). The advantage of this strategy is that atlas users can compare histology and tracing. Its major disadvantage, however, is that the 3D appearance of cerebral

regions is not verified, which can lead to 3D incoherencies as it is the case in the Schaltenbrand atlas (Niemann et al., 1994; Niemann and van Nieuwenhofen, 1999; Schaltenbrand and Wahren, 1977) and particularly regarding the STN (Dormont et al., 2004). The other strategy, the one we have chosen, consists of using the real 3D anatomy of the brain specimen, provided by its MRI, to correct for distortion that histological processing provokes. Doing this, histology is still considered as the real anatomical information but it is reconstructed in the 3D space of the original brain, leading to a 3D histological information that can be sliced in any direction while retaining spatial relationships as close as possible to those *in vivo*.

Atlas data acquisition

The initial alignment of contours based on the fiducial markers that were introduced in the brain before sectioning was not satisfactory. This is due to several distortion factors. First the entire hemisphere experienced mechanical deformation due to collapse of the lateral ventricle which involved preferentially the dorsoventral aspect of the hemisphere. This resulted in an erroneous estimation, finally corrected, of the dorsoventral and mediolateral axes. Then a global shrinkage, not quantifiable, resulted from the fixation and the freezing of the hemisphere. Finally, each section was processed separately, although in the same mixtures, and mounted separately on a lamella. Therefore, individual local deformations could occur although each section was spread on the lamella with very great care by highly trained technicians. Thus, the initial alignment of the contours based on the fiducial markers was not satisfactory and was finally abandoned to the benefit of an atlas data coregistration based on the alignment of the cryo sections with reference to the rivets of the microtome (Fig. 5).

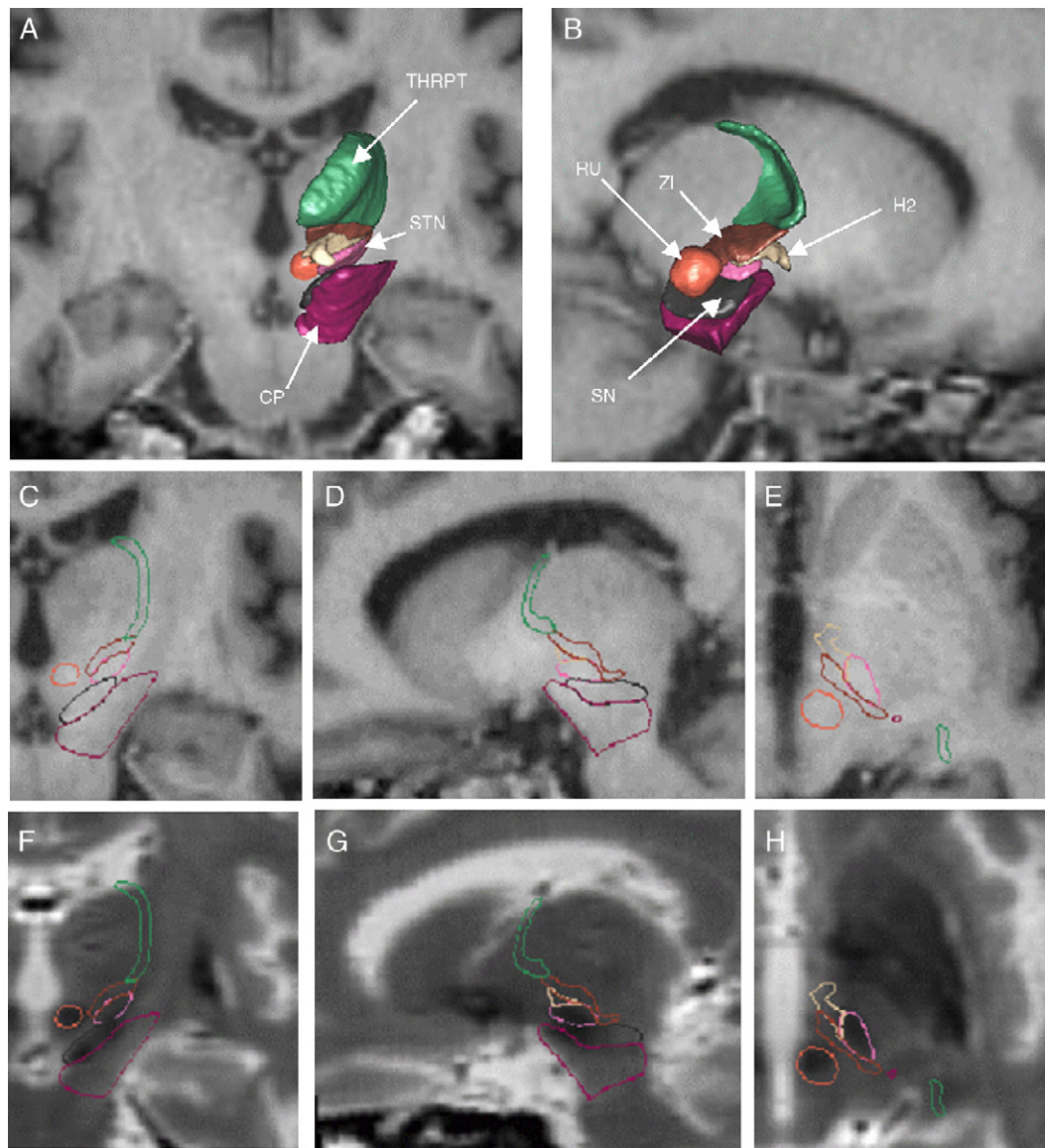


Fig. 14. Atlas surfaces of the subthalamic region: cerebral peduncle (CP), Forel's field H2 (H2), red nucleus (RU), substantia nigra (SN), subthalamic nucleus (STN), reticular perithalamic nucleus (THRPT), zona incerta (ZI) as shown in an anterior (A) and a lateral (B) view. The same structures after fusion with the T1 MRI are sectioned in the frontal (C), sagittal (D) and horizontal (E) planes. Same structures after fusion with the T2 MRI in the frontal (F), sagittal (G) and horizontal (H) planes. These sections allow to verify the 3D consistency of atlas surfaces and the adequacy with the zones of T2 hypointense signal.

Atlas data coregistration

Registration is a central problem in the medical image processing literature. Intra- or inter-patient, mono or multimodal registration has been studied extensively (Maintz and Viergever, 1998; Zitova and Flusser, 2003), but coregistration of 2D histological and 3D MRI data of the same specimen requires a specific methodology which can mimic the data acquisition protocol (Malandain et al., 2004; Mega et al., 1997; Schormann and Zilles, 1998).

Two problems had to be solved. First, 2D histological sections needed to be realigned and reconstructed as a 3D block. Second, this 3D block needed to be registered with the corresponding MRI data. As the data acquisition protocol included photographs taken during frozen brain cutting with fiducial markers (the rivets) included in the field of view, marker-based alignment of these photographs

produced intermediate 3D blocks that possess the 3D shape properties of the specimen (Malandain et al., 2004; Mega et al., 1997; Schormann and Zilles, 1998; Streicher et al., 1997). Alignment was performed using rigid transforms in order to correct for small variations of the cryomicrotome stage position during photography.

Histological 2D sections could then be realigned into 3D blocks through series of slice-by-slice cryo to histological 2D registrations. Each 2D cryo to histological registration was first initialized with a global (rigid+scaling) alignment. Histological processing can produce non-linear and slice-to-slice variable distortions. In order to compensate for these distortions, various non-linear regularization schemes combining elastic and fluid terms (Cachier et al., 2003; Stefanescu et al., 2004) were tested. These variational approaches estimate deformations with a high number of degrees of freedom and

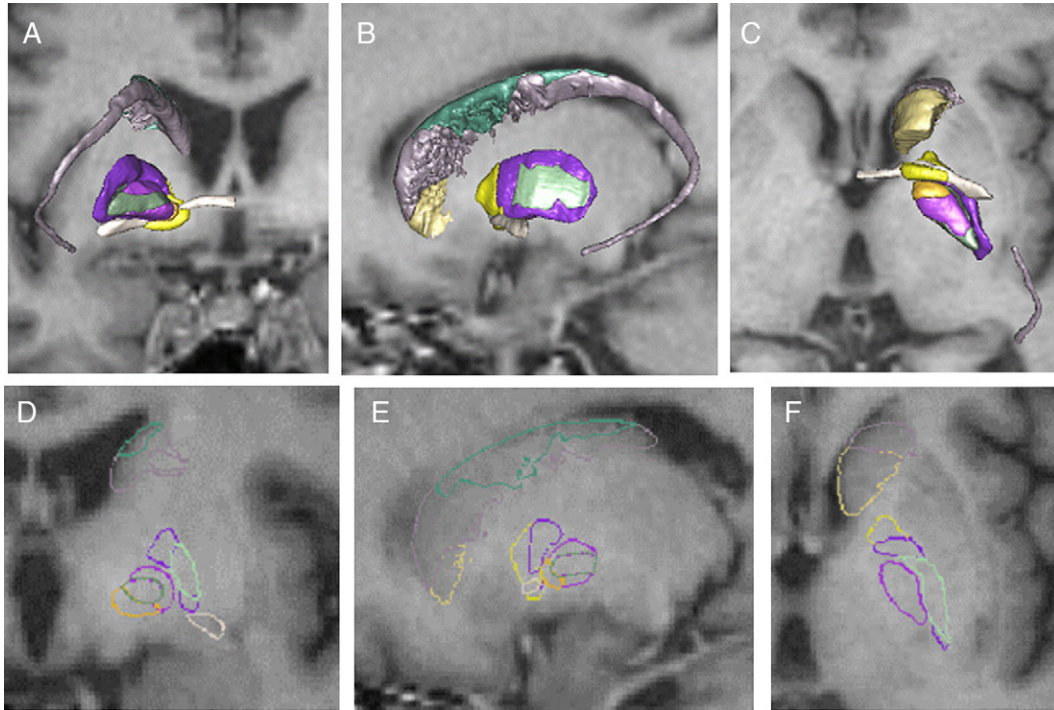


Fig. 15. The three functional territories of the caudate nucleus, putamen, external and internal globus pallidus as seen in posterior (A), lateral (B) and inferior (C) views. The same nuclei are sectioned in frontal (D), sagittal (E) and horizontal (F) planes. The anterior commissure is in white. The sensorimotor, associative and limbic territories are in green, purple and yellow, respectively. (For interpretation of the references to colour in this figure legend, the reader is referred to the web version of this article.)

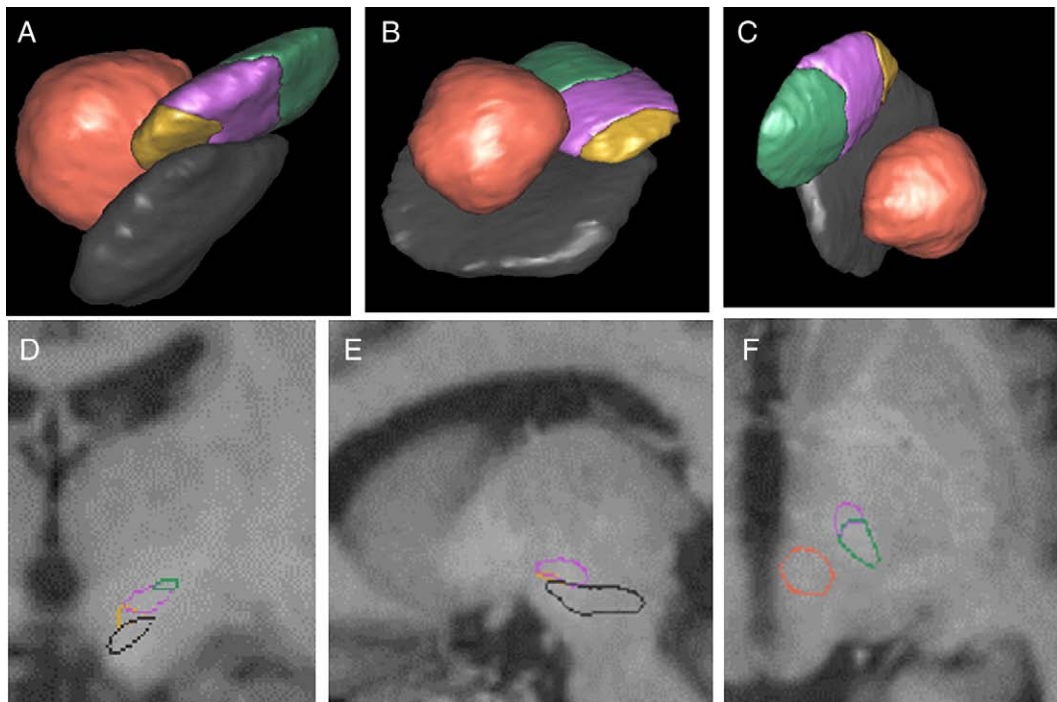


Fig. 16. The three functional territories of the subthalamic nucleus as inferred from tracing experiments in the monkey (Karachi et al., 2005). The sensorimotor territory is in green, the associative territory in purple, and the limbic territory in yellow. Anterior view (A), lateral view (B) and superior view (C) with the red nucleus (in orange) and substantia nigra (in grey). Frontal (D), sagittal (D) and horizontal (E) sections of the same structures after fusion with the T1 MRI. (For interpretation of the references to colour in this figure legend, the reader is referred to the web version of this article.)

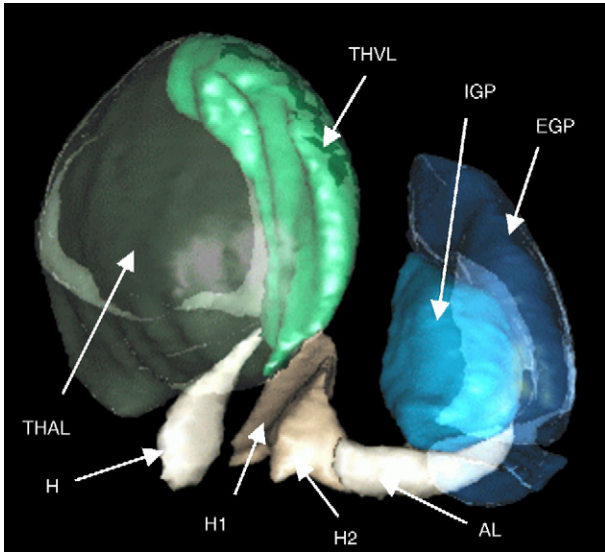


Fig. 17. Anterior view of the external (EGP) and internal globus pallidus (IGP), the ansa lenticularis (AL), Forel's fields H2, H1 and H, the entire thalamus (THAL) and its ventral lateral subdivision (THVL).

require to tune a number of parameters in order to get the best compromise between goodness-of-fit and transformation regularity. As we were strictly interested in the basal ganglia area, and not the cortical level, and as a strong constraint of our registration pipeline concerned the preservation of the anatomical information provided by the histological sections, we preferred to focus on this particular region searching for transformations with less degrees of freedom. Thus, a 3D region of interest (ROI) around the basal ganglia area was extracted from the 3D cryo block. The globally registered histological slices being stacked, the corresponding 3D ROI was also extracted, yielding pairs of cryo and histological 2D ROIs per slice. These pairs were subsequently coregistered with affine transformations. During calbindin immunohistochemistry, the histological sections were immersed several times in different mixtures and eventually suffered more distortions than Nissl-stained sections. Nevertheless, the strategy retained for atlas data coregistration allowed to get a satisfactory matching for both sections. The last

registration concerned the 3D cryo block and the MRI data. We chose the T1-weighted MRI because there was a minimal number of intermediate steps between the acquisition of these two datasets (brain extraction, fixation and freezing). Thus distortions were minimal, excepts the ventricle collapse due to CSF leak during brain extraction. As for the 2D cryo to histological registrations, global followed by ROI-based local registration scheme was applied.

Atlas data optimization

We combined cryo sectioned data, a source of high resolution stained anatomy, and an electronically acquired MRI dataset as recommended by the human brain mapping consortium (Mazziotta et al., 2001). Optimization was needed to compensate for two types of irregularities: (1) uncertainties of contour tracing which can occur in particular cerebral regions and (2) residual errors (not higher than millimetric) of the coregistration which otherwise provided good results as exemplified in Figs. 8, 13, 14 and 16). Our optimization strategy was largely based on the MRIs of the atlas because they were acquired before extraction of the brain from the skull, thus providing the real 3D anatomy of the brain specimen. Viewing the atlas surfaces into the T1 and T2 MRI provided the final and most pertinent testing of the atlas data. The contours obtained by slicing the atlas surfaces into any plane of section were expected to be at the same time smooth (without any unjustifiable irregularity) and corresponding accurately to the same structures in the MRI. This confirmation was performed for all atlas surfaces and particularly for those that were precisely discernable in the MRI, as for example the striatum (caudate nucleus and putamen) and the cerebral peduncle (ventrolateral border). The tracing of the STN, red nucleus and substantia nigra was verified with the T2 sequence acquisition of the brain atlas. In this sequence these structures appear as hypointense signals (Dormont et al., 2004), which can be used to verify their localization and orientation.

When the 3D atlas surfaces did not fit the corresponding structures in the MRI, the matching of the corresponding contours with the histological blocks was checked and modified using multimodal and 3D criteria at two correction levels: 3D smoothing and anatomical retracing. Smoothing was made in the TTS environment which enabled the anatomist (JY) to construct a tracing which took into account both the 3D consistency and the

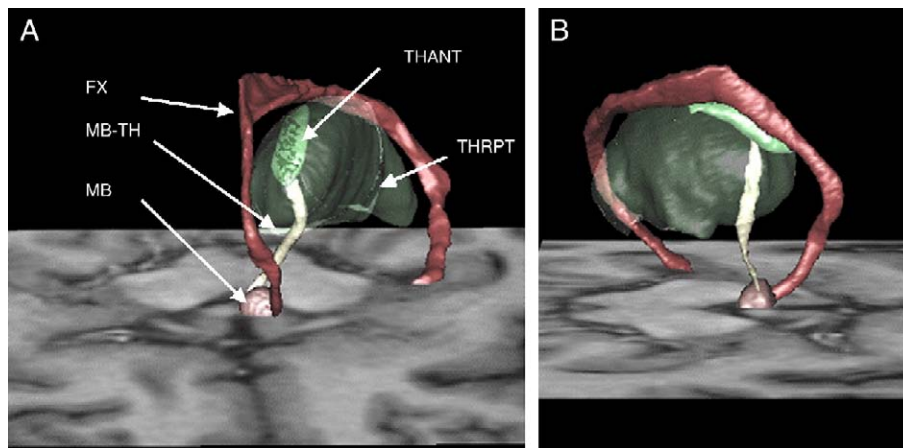


Fig. 18. Anterior (A) and lateral (B) views of the mammillary body (MB), fornix (FX), mamillothalamic tract (MB-TH), anterior thalamic nucleus (THANT) and reticular perithalamic nucleus (THRPT, with transparent rendering) after fusion with the T1 MRI. An axial plane of which is visualized.

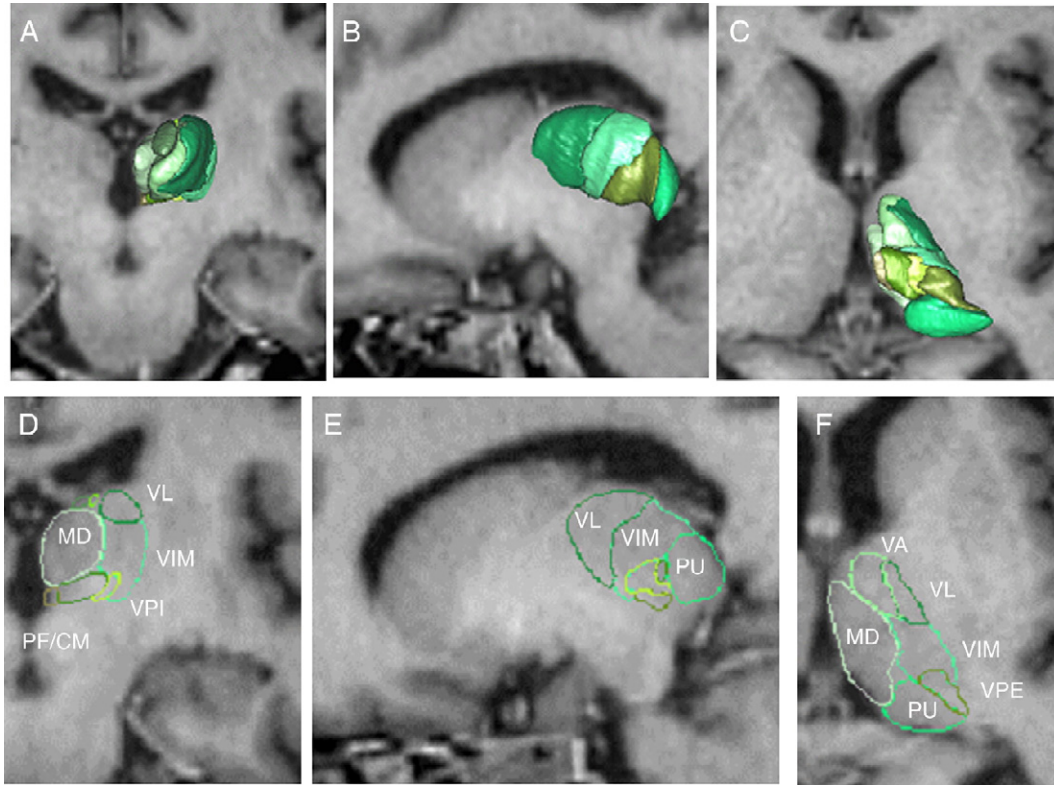


Fig. 19. Anterior (A), lateral (B) and superior (C) views and frontal (D), sagittal (E) and horizontal (F) sections of the main thalamic nuclei: ventral anterior (VA), ventral lateral (VL), ventralis intermedius (VIM), ventral posterior internal (VPI) and external (VPE), mediodorsal (MD), pulvinar (PU), centre median parafascicular complex (PF/CM).

histological truth. Anatomical retracing was necessary when larger inconsistencies were observed. One cause was attributed to residual errors of the coregistration, as for example for the tail of the caudate nucleus (black arrow for CD in Fig. 9) which was located at the periphery of the ROI used during coregistration. Another cause was due to uncertainties of the initial tracing, such as for the ventral border of the globus pallidus (black arrow for EGP in Fig. 9), whose frontier with the nucleus basalis is known to be fuzzy (Karachi et al., 2002). Optimized tracings were considered as more reliable as they were validated on several adjacent histological sections and had a 3D consistency.

Contours of the mammillary body, fornix and anterior part of the optic tract had to be traced directly on the MRIs when they were not visible in histological sections (fornix in Fig. 7). Accuracy of these particular tracings was therefore limited to the MRI pixel size (1 mm^3) unlike the other atlas contours which had a histological level of resolution.

Basal ganglia functional subdivisions

A significant novel feature of the atlas is that it includes functional subdivisions of the basal ganglia. These subdivisions are based on the nature of the cortical information that is processed in different regions of the basal ganglia. Tracing experiments in the monkey have demonstrated that the primary somatosensory, primary motor, premotor and oculomotor cortices project mainly to the putamen in the form of three somatotopic strips corresponding to the arm, face and leg (Flaherty and Graybiel, 1994; Künzle, 1975; Percheron et al., 1984). This subdivision which processes senso-

rimotor information is referred to as the sensorimotor territory. A second subdivision arises from the prefrontal, posterior parietal and temporal associative cortices and terminates mainly in the caudate nucleus without any clear-cut somatotopic organization (Selemon and Goldman-Rakic, 1985; Yeterian and Pandya, 1991). This subdivision, referred to as the associative territory, processes cognitive information. A third subdivision arises from the anterior cingulate, orbitofrontal limbic and paralimbic cortices and from the amygdala and hippocampus and projects to the ventral part of the caudate nucleus and putamen known as the nucleus accumbens (Kunishio and Haber, 1994; Parent and Hazrati, 1995; Russchen et al., 1985). This subdivision, referred to as the limbic territory, processes emotional and motivational information. These three functional territories, identified in the cortico-striatal projection, are maintained through the projection from the striatum to the globus pallidus and substantia nigra.

In the basal ganglia of monkey, a parallelism has been demonstrated between the topography of these projections and the distribution of the calcium-binding protein calbindin: the sensorimotor territory is not immunoreactive to calbindin while the associative territory exhibits a positive reactivity and the limbic territory a strong immunoreactivity (François et al., 1994). Examination of large series of monkey brains in our laboratory (François et al., 1994, 1996, 2004; Jan et al., 2000) revealed that the distribution of calbindin staining was largely similar from one individual to another. More precisely, the strongly labeled limbic territory was always found in the ventral portion of the striatum while the non-labeled sensorimotor portion was always localized in the putamen. In the human it is not possible to demonstrate the topography of the

cortico-striatal projection by tracing experiments but as the distribution of calbindin is similar to that observed in the monkey, it has been considered as a marker of the associative and limbic territories in the human, with a topographic distribution highly similar to that observed in the monkey (Holt et al., 1997; Karachi et al., 2002). In the present atlas the limits between the three functional territories have been traced as numerical data, leading to sharply defined territories. In reality, these limits are not clear cut and in fact correspond to progressive gradients of cortical projections (Karachi et al., 2002). Moreover, it is likely that interindividual variations in the size of each territory exist. Users must thus recognize that

individual variations in localization of the boundaries of the functional subdivisions are likely to be on the order of several millimeters.

The functional subdivision of the STN raised particular questions because this nucleus is not immunoreactive to calbindin, although limbic and associative subdivisions have been described in the monkey based on tracing experiments (Karachi et al., 2005). In the absence of a specific marker of the functional subdivision of the STN, it was considered that the 3D topography of the three territories was similar in the monkey and the human STN. This prediction is supported by observations showing that motor and

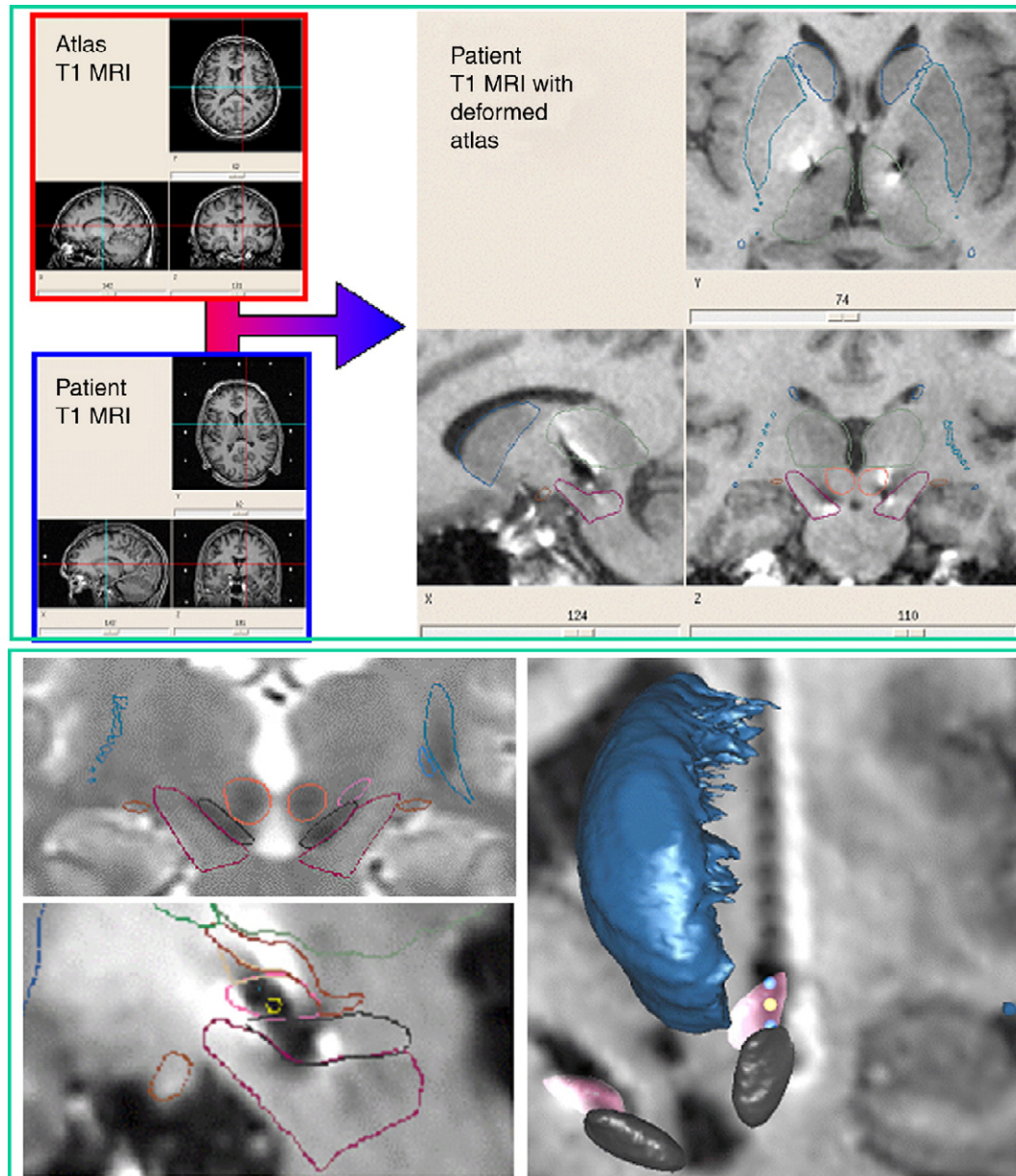


Fig. 20. Atlas adaptation onto a patient's MRI. Upper box: Atlas deformation is obtained by automatic coregistration between atlas and patient T1 MRIs. Lower box: Application of the deformable atlas for deep brain stimulation of a parkinsonian patient. Upper left: Atlas contours in a frontal preoperative T2 slice. Lower left: Atlas contours in a sagittal postoperative T1 slice. Right: 3D image oriented along the axis of the electrode with the caudate nucleus in blue, the subthalamic nucleus in pink, the substantia nigra in black. The active contact is yellow, the other ones are blue. Note the good correspondence between atlas contours and MRI structures in the two planes of section and the localization of the active electrode contact (yellow circle) within the intended target (subthalamic nucleus). (For interpretation of the references to colour in this figure legend, the reader is referred to the web version of this article.)

mood responses are obtained by stimulation of different parts of the STN in human parkinsonian patients (MacKinnon et al., 2005; Mallet et al., 2002; Stefurak et al., 2003). However, it must be remembered that the relative size of the territories could be different in the two species.

Atlas adaptation onto individual patients

As a proof of concept, deformation of atlas surfaces onto a patient's MRI is illustrated in Fig. 20. Deformation has been obtained by automatic coregistration of the atlas and patient's MRI volumes following a hierarchical framework consisting of an initial alignment of the two volumes by applying the BALADIN algorithm to the entire heads, and refinement of the deformation by local registration of ROIs defined around basal ganglia structures. The atlas was deformed independently on each hemisphere of the patient. The exact procedure with which the atlas surfaces are deformed to fit the geometry of each patient's brain has been published in the peer reviewed MICCAI conference (Bardinet et al., 2005) and will be described in a forthcoming paper together with an evaluation on a series of parkinsonian patients. The evaluation will include a comparison between localization of basal ganglia structures given by the 3D atlas and the identification of the same structures based on intra-operative micro-electrode recordings, and a comparison with previous atlas studies based on the most frequently used Schaltenbrand and Wahren atlas.

Conclusion

As far as we know, the atlas that we have developed is the only one in which anatomical contours have been traced at the histological level of resolution but for which 3D coherency has been given major focus. The successive steps of the construction of this atlas include manual processing for data acquisition, automated processing for data coregistration and semi-automatic processing under manual control for data optimization. This explains why the entire process of the atlas construction has extended over a work period of several years during which several procedures of histological brain processing and medical image processing were designed, tested and optimized. In our opinion this important effort is justified since with such a 3D atlas, sectioning of the resulting surfaces provides smooth and relevant contours whatever the orientation of the plane of section. In particular, this can be used to analyze the cerebral structures which are crossed through with an obliquely oriented trajectory such as a biopsy or a deep brain stimulation electrode.

Based on the present results and the forthcoming evaluation paper, we conclude that a 1 mm accuracy for target localization in individual patients will be achievable with this atlas. This atlas and deformation procedure will have the potential to become a generally applicable clinical tool in DBS protocols and other clinical situations in which identification of the basal ganglia with a high degree of resolution is required.

Acknowledgments

This work was supported by grant Medtronic 97506 and FRC 2005. We thank Professor Lassau (Institut d'Anatomie, Université Paris V) who provided the autopsy specimen. Special thanks are expressed to Doctor David Seidenwurm who kindly made an attentive revision of the English of the manuscript.

Appendix A. Three-dimensional Tracing Software application (TTS)

This was developed in the INSERM group and allows the tracing of contours via a Summa sketch III (SummaGraphic) XY digitizer, their storage in a database and their interactive optimization. Each histological section is stored in a "section file" which contains all the contours traced in this section. Each contour is identified by an alphanumeric label and stored in the form of X and Y coordinates. A "brain file" contains the list of all the sections digitized in a given brain and their localization within the entire brain (e.g. the anteriority with reference to the PC point for frontal sections). A cerebral region is digitized as a set of contours traced in different histological sections.

The following tools of the TTS have been particularly useful in this study. Contours can be visualized in the point and/or vector mode and individual points can be modified interactively on the screen display using the mouse. Sections can be visualized successively allowing to progress rostral ward or caudal ward within cerebral regions. The contours of a given cerebral region in individual sections can be identified with a specific color. Two sections adjacent to a given section – the two closest sections, the two Nissl closest, the two calbindin closest or any two sections – can be displayed in different colors (Fig. 10). In the adjacent sections mode, visualization of successive sections displays the three adjacent sections at each pressing of the button. The zoom function which allows to examine a part of a section or a restricted portion of a given contour, can be applied in the single section or the adjacent sections mode. A contour can be traced by duplication of a portion of another contour traced previously if their limits are superposed. In the point modification mode, duplicated points can be modified simultaneously or separately. A cerebral region can be viewed in a smooth rotation around the X or Y axis with an adjustable step (from a fraction of degree to several degrees). Several cerebral regions can be rotated simultaneously with different colors (Fig. 12). A zoom can be applied during rotation on a particular portion of the scene. One or several cerebral regions can be sliced in the sagittal plane with an adjustable thickness of the slice (Fig. 9). A given contour or all the contours of a given section can be translated, rotated, reduced or enlarged.

Appendix B. Yav++ software application

The Yav++ software package has been developed by the Epidaure group at INRIA (Delingette et al., 2001). It is based on a C++ library embedded in Tcl/Tk interactive tools, and it includes image processing and visualization tools. The following tools have been particularly useful in this study. Viewing of a 3D image in three orthogonal planes and navigation uses a 3D cursor. Comparison of two images previously registered by visualization of each image in a 3D viewer and navigation with a synchronized cursor that can be positioned simultaneously on the same voxel of the two images. Fusion of two images previously registered by superimposition of the two 3D images and visual appreciation of the quality of the fusion by tuning the opacity of one image relative to the other. Simultaneous visualization of 3D surfaces and image planes which allows in particular to evaluate the relative positions of different structures with regard to 3D images. The surfaces can also be reported in the 3D viewer, yielding 2D contours in each of the three orthogonal planes.

Appendix C. BALADIN software application

Starting with a reference image I and a floating image J , this algorithm aims to estimate a transformation T such as $J \circ T$ can be superimposed on I . This is done through an iterative scheme embedded in a multiscale framework. For a given scale, an iteration consists in a search of correspondences which are computed with a block matching strategy, followed by the estimation of the current transformation. Therefore, the final transformation T is computed iteratively. During the first scales, a rough approximation of the transformation is estimated, whereas the last scales allow to refine T . The block matching strategy starts with a parcellation of images I and J into subimages (blocks). Correspondences are then established between these blocks using an intensity-based similarity measure. Precisely, for a given block in image J , a series of blocks in the neighbourhood of this block in image I is explored (i.e. the similarity measure is computed), and the block giving the best measure is retained (i.e., a correspondence is established between the centers of the blocks in images I and J). This is repeated for all blocks in image J , up to the obtainment of a vector field between images I and J . In practice, as the block matching is embedded in a multiscale framework, block size is constant (5×5 voxels in 2D, $5 \times 5 \times 5$ voxels in 3D) through all scales. The choice of the similarity measure should depend on the expected relationship between the block intensities. Considering that a block may contain up to two (and rarely three) different tissues, an affine relationship seems reasonable. Hence, we choose the correlation coefficient as similarity measure (Roche et al., 2000). The transformation is computed with the least trimmed squares estimator, which is robust up to 50% of outliers present in the vector field.

References

- Afshar, F., Watkins, E.S., Yap, J.C., 1978. Stereotaxic atlas of the human brain-stem and cerebellar nuclei. A Variability Study. Raven Press, New York.
- Andrew, J., Watkins, E.S., 1969. A Stereotaxic Atlas of The Human Thalamus and Adjacent Structures. Williams and Wilkins, Baltimore.
- Bardinet, E., Ourselin, S., Dormont, D., Malandain, G., Tandé, D., Parain, K., Ayache, N., Yelnik, J., 2002a. Co-registration of histological, optical and MR data of the human brain. In: Dohi, T., Kikinis, R. (Eds.), MICCAI 2002, LNCS 2488. Springer Verlag, Berlin, pp. 548–555.
- Bardinet, E., Ourselin, S., Malandain, G., Tandé, D., Parain, K., Ayache, N., Yelnik, J., 2002b. Three dimensional functional cartography of the human basal ganglia by registration of optical and histological serial sections. IEEE. International Symposium on Biomedical Imaging Washington, USA.
- Bardinet, E., Dormont, D., Malandain, G., Bhattacharjee, M., Saleh, C., Cornu, P., Ayache, N., Agid, Y., Yelnik, J., 2005. Retrospective Cross-Evaluation of an Histological and Deformable 3D Atlas of the Basal Ganglia on Series of Parkinsonian Patients Treated by Deep Brain Stimulation. MICCAI 2005, LNCS 3750. Springer Verlag, Berlin, pp. 385–393.
- Bejjani, B.P., Dormont, D., Pidoux, B., Yelnik, J., Damier, P., Arnulf, I., Bonnet, A.M., Marsault, C., Agid, Y., Philippon, J., Cornu, P., 2000. Bilateral subthalamic stimulation for Parkinson's disease by using three-dimensional stereotactic magnetic resonance imaging and electrophysiological guidance. J. Neurosurg. 92, 615–625.
- Benabid, A.L., Pollak, P., Louveau, A., Henry, S., De Rougemont, J., 1987. Combined (thalamotomy and stimulation) stereotactic surgery of the VIM thalamic nucleus for bilateral Parkinson disease. Appl. Neurophysiol. 50, 344–346.
- Besl, P.J., McKay, N.D., 1992. A method for registration of 3-D shapes. IEEE Trans. Pattern Anal. Mach. Intell. 14, 239–256.
- Cachier, P., Bardinet, E., Dormont, D., Pennec, X., Ayache, N., 2003. Iconic feature based nonrigid registration: the PASHA algorithm. CVIU 89, 272–298 (Special Issue on Nonrigid Registration).
- Delingette, H., Bardinet, E., Rey, D., Lemarechal, J.D., Montagnat, S., Ourselin, S., Roche, A., Dormont, D., Yelnik, J., Ayache, N., 2001. Yav++: A software platform for medical image processing and visualization. Workshop on Interactive Medical Image Visualization and Analysis. Satellite symposia of MICCAI. Utrecht, The Netherlands.
- Dormont, D., Cornu, P., Pidoux, B., Bonnet, A.M., Biondi, A., Oppenheim, C., Hasboun, D., Damier, P., Cuchet, E., Philippon, J., Agid, Y., Marsault, C., 1997. Chronic thalamic stimulation with three-dimensional MR stereotactic guidance. AJNR 18, 1093–1107.
- Dormont, D., Ricciardi, K.G., Tandé, D., Parain, K., Menuel, C., Galanaud, D., Navarro, S., Cornu, P., Agid, Y., Yelnik, J., 2004. Is the subthalamic nucleus hypointense on T2-weighted images? A correlation study using MR imaging and stereotactic atlas data. AJNR 25, 1516–1523.
- Duvernoy, H.M., 2004. The Human Brain. Surface, Three-Dimensional Sectional Anatomy and MRI.
- Flaherty, A.W., Graybiel, A.M., 1994. Input–output organization of the sensorimotor striatum in the squirrel monkey. J. Neurosci. 14, 599–610.
- François, C., Yelnik, J., Percheron, G., Tandé, D., 1994. Calbindin D-28k as a marker for the associative cortical territory of the striatum in macaque. Brain Res. 633, 331–336.
- François, C., Yelnik, J., Percheron, G., 1996. A stereotaxic atlas of the basal ganglia in macaques. Brain Res. Bull. 41, 151–158.
- François, C., Grabli, D., McCairn, K., Jan, C., Karachi, C., Hirsch, E.C., Feger, J., Tremblay, L., 2004. Behavioural disorders induced by external globus pallidus dysfunction in primates: II. Anatomical study. Brain 127, 2055–2070.
- Herman, G.T., Zheng, J., Bucholtz, C.A., 1992. Shape-based interpolation. IEEE Comput. Graph. Appl. 12, 69–79.
- Holt, D.J., Graybiel, A.M., Saper, C.B., 1997. Neurochemical architecture of the human striatum. J. Comp. Neurol. 384, 1–25.
- Jan, C., François, C., Yelnik, J., Tandé, D., Agid, Y., Hirsch, E.C., 2000. Dopaminergic innervation of the pallidum in the normal state, MPTP-treated monkeys and parkinsonian patients. Eur. J. Neurosci. 12, 4525–4535.
- Karachi, C., Francois, C., Parain, K., Bardinet, E., Tande, D., Hirsch, E., Yelnik, J., 2002. Three-dimensional cartography of functional territories in the human striatopallidal complex by using calbindin immunoreactivity. J. Comp. Neurol. 450, 122–134.
- Karachi, C., Yelnik, J., Tande, D., Tremblay, L., Hirsch, E.C., Francois, C., 2005. The pallidum-subthalamic projection: an anatomical substrate for nonmotor functions of the subthalamic nucleus in primates. Mov. Disord. 20, 172–180.
- Kunishio, K., Haber, S.N., 1994. Primate cingulo-striatal projection: limbic striatal versus sensorimotor striatal input. J. Comp. Neurol. 350, 337–356.
- Künzle, H., 1975. Bilateral projections from precentral motor cortex to the putamen and other parts of the basal ganglia. An autoradiographic study in *Macaca fascicularis*. Brain Res. 88, 195–209.
- Limousin, P., Pollak, P., Benazzouz, A., Hoffmann, D., Broussolle, E., Perret, J.E., Benabid, A.L., 1995. Bilateral subthalamic nucleus stimulation for severe Parkinson's disease. Mov. Disord. 10, 672–674.
- MacKinnon, C.D., Webb, R.M., Silberstein, P., Tisch, S., Asselman, P., Limousin, P., Rothwell, J.C., 2005. Stimulation through electrodes implanted near the subthalamic nucleus activates projections to motor areas of cerebral cortex in patients with Parkinson's disease. Eur. J. Neurosci. 21, 1394–1402.
- Mai, J.K., Assheuer, J., Paxinos, G., 1997. Atlas of the Human Brain. Academic Press, San Diego, pp. 1–328.
- Maintz, J.B., Viergever, M.A., 1998. A survey of medical image registration. Med. Image Anal. 2, 1–36.
- Malandain, G., Bardinet, E., 2003. Intensity compensation within series of

- images. In: Ellis, R.E., Peters, T.M. (Eds.), *MICCAI 2003*, LNCS 2879. Springer Verlag, Montreal, pp. 41–49.
- Malandain, G., Bardinet, E., Nelissen, K., Vanduffel, W., 2004. Fusion of autoradiographs with an MR volume using 2-D and 3-D linear transformations. *NeuroImage* 23, 111–127.
- Mallet, L., Mesnage, V., Houeto, J.L., Pelissolo, A., Yelnik, J., Behar, C., Gargiulo, M., Welter, M.L., Bonnet, A.M., Pillon, B., Cornu, P., Dormont, D., Pidoux, B., Allilaire, J.F., Agid, Y., 2002. Compulsions, Parkinson's disease, and stimulation. *Lancet* 360, 1302–1304.
- Mazziotta, J., Toga, A., Evans, A., Fox, P., Lancaster, J., Zilles, K., Woods, R., Paus, T., Simpson, G., Pike, B., Holmes, C., Collins, L., Thompson, P., MacDonald, D., Jacoboni, M., Schormann, T., Amunts, K., Palomero-Gallagher, N., Geyer, S., Parsons, L., Narr, K., Kabani, N., Le Goualher, G., Boomsma, D., Cannon, T., Kawashima, R., Mazoyer, B., 2001. A probabilistic atlas and reference system for the human brain: International Consortium for Brain Mapping (ICBM). *Philos. Trans. R. Soc. Lond., B Biol. Sci.* 356, 1293–1322.
- Mega, M.S., Chen, S.S., Thompson, P.M., Woods, R.P., Karaca, T.J., Tiwari, A., Vinters, H.V., Small, G.W., Toga, A.W., 1997. Mapping histology to metabolism: coregistration of stained whole-brain sections to premortem PET in Alzheimer's disease. *NeuroImage* 5, 147–153.
- Menual, C., Garnero, L., Bardinet, E., Poupon, F., Dormont, D., 2005. Characterization and correction of geometric distortions in stereotactic MRI for bilateral subthalamic stimulation in Parkinson disease. *J. Neurosurg.* 103, 256–266.
- Morel, A., Magnin, M., Jeanmonod, D., 1997. Multiarchitectonic and stereotactic atlas of the human thalamus. *J. Comp. Neurol.* 387, 588–630.
- Niemann, K., van Nieuwenhofen, I., 1999. One atlas—three anatomies: relationships of the Schaltenbrand and Wahren microscopic data. *Acta Neurochir. (Wien.)* 141, 1025–1038.
- Niemann, K., Naujokat, C., Pohl, G., Wollner, C., von Keyserlingk, D., 1994. Verification of the Schaltenbrand and Wahren stereotactic atlas. *Acta Neurochir. (Wien.)* 129, 72–81.
- Niemann, K., Mennicken, V.R., Jeanmonod, D., Morel, A., 2000. The Morel stereotactic atlas of the human thalamus: atlas-to-MR registration of internally consistent canonical model. *NeuroImage* 12, 601–616.
- Ourselin, S., Roche, A., Prima, S., Ayache, N., 2000. Block matching: a general framework to improve robustness of rigid registration of medical images. In: DiGioia, A.M., Delp, S. (Eds.), *Third International Conference on Medical Robotics, Imaging And Computer Assisted Surgery (MICCAI 2000)*. Springer, Pittsburgh, PA, USA, pp. 557–566.
- Ourselin, S., Bardinet, E., Dormont, D., Malandain, G., Roche, A., Ayache, N., Tandé, D., Parain, K., Yelnik, J., 2001. Fusion of histological sections and MR images: towards the construction of an atlas of the human basal ganglia. In: Niessen, W., Viergever, M. (Eds.), *MICCAI 2001*, LNCS 2208. Springer Verlag, Berlin, pp. 743–751.
- Parent, A., 1990. Extrinsic connections of the basal ganglia. *Trends Neurosci.* 13, 254–258.
- Parent, A., Hazrati, L.N., 1995. Functional anatomy of the basal ganglia: 1. The cortico-basal ganglia-thalamo-cortical loop. *Brain Res. Rev.* 20, 91–127.
- Percheron, G., Yelnik, J., François, C., 1984. A Golgi analysis of the primate globus pallidus: III. Spatial organization of the striato-pallidal complex. *J. Comp. Neurol.* 227, 214–227.
- Percheron, G., François, C., Talbi, B., Yelnik, J., Fénelon, G., 1996. The primate motor thalamus. *Brain Res. Rev.* 22, 93–181.
- Prima, S., Ourselin, S., Ayache, N., 2002. Computation of the mid-sagittal plane in 3D brain images. *IEEE Trans. Med. Imaging* 21, 122–138.
- Roche, A., Malandain, G., Ayache, N., 2000. Unifying maximum likelihood approaches in medical image registration. *Int. J. Imaging Syst. Technol.* 11 (1), 71–80 (Special Issue on 3D Imaging).
- Russchen, F.T., Bakst, I., Amaral, D.G., Price, J.L., 1985. The amygdalo-striatal projections in the monkey. An anterograde tracing study. *Brain Res.* 329, 241–257.
- Schaltenbrand, G., Bailey, P., 1959. *Introduction to Stereotaxis with an Atlas of the Human Brain*. Georg thieme Verlag, Stuttgart.
- Schaltenbrand, G., Wahren, W., 1977. *Atlas for Stereotaxy of the Human Brain*. Georg Thieme Verlag, Stuttgart.
- Schormann, T., Zilles, K., 1998. Three-dimensional linear and nonlinear transformations: an integration of light microscopical and MRI data. *Hum. Brain Mapp.* 6, 339–347.
- Selemon, L.D., Goldman-Rakic, P.S., 1985. Longitudinal topography and interdigitation of corticostriatal projections in the rhesus monkey. *J. Neurosci.* 5, 776–794.
- Stefanescu, R., Pennec, X., Ayache, N., 2004. Grid powered nonlinear image registration with locally adaptive regularization. *Med. Image Anal.* 8, 325–342.
- Stefurak, T., Mikulis, D., Mayberg, H., Lang, A.E., Hevenor, S., Pahapill, P., Saint-Cyr, J., Lozano, A., 2003. Deep brain stimulation for Parkinson's disease dissociates mood and motor circuits: a functional MRI case study. *Mov. Disord.* 18, 1508–1516.
- Streicher, J., Weninger, W.J., Muller, G.B., 1997. External marker-based automatic congruencing: a new method of 3D reconstruction from serial sections. *Anat. Rec.* 248, 583–602.
- Talairach, J., Tournoux, P., 1988. *Co-Planar Stereotaxic Atlas of the Human Brain*. Thieme Medical Publishers, Inc., New York.
- Talairach, J., David, M., Tournoux, P., Corredor, H., Kvasina, T., 1957. *Atlas d'Anatomie Stéréotaxique*. Masson and Compagnie, Paris.
- Van Buren, J.M., Borke, R.C., 1972. *Variations and Connections of the Human Thalamus*. Springer, Berlin.
- Yelnik, J., Damier, P., Bejjani, B.P., François, C., Gervais, D., Dormont, D., Arnulf, I., Bonnet, A.M., Cornu, P., Pidoux, B., Agid, Y., 2000. Functional mapping of the globus pallidus. Contrasting effect of stimulation in the internal and external pallidal nuclei in Parkinson's disease. *Neuroscience* 101, 77–87.
- Yelnik, J., Damier, P., Demeret, S., Gervais, D., Bardinet, E., Bejjani, B.P., François, C., Houeto, J.L., Arnulf, I., Dormont, D., Galanaud, D., Pidoux, B., Cornu, P., Agid, Y., 2003. Localization of stimulating electrodes in parkinsonian patients by using a three-dimensional atlas—magnetic resonance imaging coregistration method. *J. Neurosurg.* 99, 83–93.
- Yeterian, E.H., Pandya, D.N., 1991. Prefrontostriatal connections in relation to cortical architectonic organization in rhesus monkeys. *J. Comp. Neurol.* 312, 43–67.
- Zitova, B., Flusser, J., 2003. Image registration methods: a survey. *Image Vis. Comput.* 21, 977–1000.